Application of the SAFT-γ Mie group contribution equation of state to fluids of relevance to the oil and gas industry

Vasileios Papaioannou[a], Filipe Calado[b], Thomas Lafitte[b], Simon Dufal[a], Majid Sadeqzadeh[a], George Jackson[a], Claire S. Adjiman[a], Amparo Galindo[a,*]

[a]*Department of Chemical Engineering, Centre for Process Systems Engineering, Imperial College London, SW7 2AZ, United Kingdom*
[b]*Process Systems Enterprise Ltd., 5th Floor East, 26-28 Hammersmith Grove, London, W6 7HA, United Kingdom*

Abstract

The application of the SAFT-γ Mie group contribution approach [Papaioannou *et al.*, *J. Chem. Phys.*, 140 (2014) 054107] to the study of a range of systems of relevance to the oil and gas industry is presented. In particular we consider carbon dioxide, water, methanol, aromatics, alkanes and their mixtures. Following a brief overview of the SAFT-γ Mie equation of state, a systematic methodology for the development of like and unlike group parameters relevant to the systems of interest is presented. The determination of group-group interactions entails a sequence of steps including: the selection of representative components and mixtures (in this instance carbon dioxide, water, methanol, aromatics and alkanes); the definition of an appropriate set of groups to describe them; the collection of target experimental data used to estimate the group-group interactions; the determination of the group-group interaction parameters; and the assessment of the adequacy of the parameters and theoretical approach. The predictive capability of the SAFT-γ Mie group contribution approach is illustrated for a selection of mixtures, including representative examples of the simultaneous description of vapour-liquid and liquid-liquid equilibria, the densities of the coexisting phases, second derivative thermodynamic properties, and excess properties of mixing. Good quantitative agreement between the predictions and experimental data is achieved, even in the case of challenging mixtures comprising carbon dioxide and water, n-alkanes and water, and methanol and methane.

Keywords: SAFT-VR, SAFT, group contribution methods, oil and gas, fluid-phase behaviour

1. Introduction

Thermodynamic methodologies are applied extensively in broad sectors of the chemical industry, alongside experimental validation, for the prediction of property of highly complex fluids and fluid mixtures. A plethora of models are available, and numerous reviews have been published on the industrial requirements

*Corresponding author
    Email address:* `a.galindo@imperial.ac.uk` (Amparo Galindo)

for the development of high-fidelity methodologies that can be used for the accurate prediction of properties of an ever-increasing range of substances, relevant to the oil and gas, chemical and pharmaceutical industries.The oil and gas sector in particular has long been a driver for the development of classes of equations of state applicable to real systems, such as the Peng-Robinson equation (PR) [1], the Soave-Redlich-Kwong equation (SRK) [2], the cubic-plus-association equation (CPA) [3], and the statistical associating fluid theory (SAFT) [4, 5]. In recent years, there has been increasing focus on predictive equations of state, such as the predictive PR2SRK [6], predictive Peng-Robinson PPR78 [7], and SAFT methods incorporating group-contribution concepts [8–13] with a view to deliver accurate predictions of properties for an ever-increasing range of systems.

Thermodynamic models are routinely employed in the design and optimization of separation and production processes, where the accuracy of the model can greatly impact the design of the process [14, 15]. The systems typically encountered in the context of the oil and gas industry include mixtures of water, carbon dioxide, hydrocarbons comprising aliphatic and aromatic components, and in some cases alcohols used as hydrate inhibitors [16]. These systems are highly non-ideal and the accurate modelling of their fluid-phase behaviour, which can include vapour-liquid and liquid-liquid equilibria, is a challenging task.

Crude oil can contain thousands of different components, not all of which can be considered specifically, and the capability of thermodynamic models to treat multicomponent mixtures predictively is an important consideration in model development in this context. As a result, the suitability of a thermodynamic methodology is judged in part based on its success in predicting the fluid-phase behaviour of multicomponent mixtures based on a limited set of binary interaction parameters. Another consideration is the modelling of the fluid-phase behaviour and properties of mixtures in the vicinity of the critical region, especially in systems comprising carbon dioxide, that has a critical point at near-ambient temperature ($T_{\mathrm{crit,CO_2}} = 304.13$ K, $P_{\mathrm{crit,CO_2}} = 7.372$ MPa [17]). While considerable effort has been devoted to the prediction of the fluid-phase behaviour of binary and multi-component mixtures, several aspects of the application of thermodynamic models to the oil and gas industry warrant more attention. As summarized by Kontogeorgis and Folas [18] in their excellent book, these include the prediction of caloric properties (i.e., heats of mixing and heat capacities) over a range of thermodynamic conditions and the prediction of a variety of properties that are important for fluid-flow calculations from equations of state (e.g., densities, speed of sound, etc.).

A single thermodynamic modelling framework would ideally provide an accurate description of all of the relevant properties for the systems of interest in the oil and gas sector over a broad range of conditions. In current industrial practice, however, cubic equations of state (EoSs) such as the Redlich-Kwong (RK) [19], the SRK [2], or the PR [1] equations are often used for the study of non-aqueous mixtures (e.g., mixtures of carbon dioxide and hydrocarbons) while more sophisticated approaches that explicitly account for association (e.g., variants of the statistical associating fluid theory (SAFT) [4, 5, 20, 21], or the cubic-plus-association (CPA) EoS [3]) are applied for the study of more complex mixtures, including aqueous solutions, and

2

mixtures containing methanol and/or other alcohols.

The application of thermodynamic methodologies to the modelling of systems of relevance to the oil and gas industry has been the subject of numerous studies. The performance of the most popular modifications of the van der Waals EoS, the RK [19], SRK [2], and PR [1] variants, in the description of the phase behaviour and volumetric properties of mixtures of carbon dioxide with alkanes has been extensively studied [22, 23]. While these methods can provide a very good description of the compositions and pressure of the fluid-phase equilibria of binary and multicomponent mixtures of hydrocarbons, carbon dioxide, and other gases, the volumetric properties of these systems are not described as accurately; this can be addressed to some extent by employing volume-translation methods [24]. Moreover, in order to achieve an accurate representations of the properties of multi-component mixtures, a considerable amount of experimental data is required for the determination of the binary interaction parameters between each of the binary pairs of components in a given mixture. In an effort to overcome the reliance on experimental data, and with the aim of developing more predictive approaches, extensions of the classical cubic equations of state have been developed. The predictive Peng-Robinson (PPR78) [7] and the PR2SRK [6] EoSs are, perhaps, the best known. In these approaches the unlike intermolecular binary interaction parameters are determined based on the different chemical groups the molecules comprise. The PPR78 EoS has been applied to describe the fluid-phase behaviour of mixtures of carbon dioxide and alkanes [25], as well as of aqueous solutions of hydrocarbons and carbon dioxide [26], where the capability of the EOSs was demonstrated in the description of the fluid-phase behaviour and excess enthalpies of mixing (using temperature-dependent interaction parameters). These studies did not include the prediction of the excess volume of mixing and other thermodynamic properties that relate to the compressibility of fluids, such as the isothermal compressibility or the speed of sound [27].

When the focus is the description of the fluid-phase behaviour of systems of components which hydrogen bond or are strongly polar, more sophisticated methods, such as the statistical associating fluid theory SAFT [4, 5] or the cubic-plus-association (CPA) EoS [3] are recommended. These thermodynamic approaches are particularly suited for the description of fluid-phase behaviour in associating systems, as they account explicitly for the presence of directional interactions. Numerous examples have been reported demonstrating the capability of several variants of the SAFT and CPA EoSs to describe accurately the highly non-ideal phase behaviour characteristic of associating systems such as aqueous solutions of hydrocarbons, or mixtures of methanol with hydrocarbons [28–35]. In general, both approaches require pure-component parameters specific to each species and appropriate binary interaction parameters need to be determined for the characterization of mixtures. This laborious process can be alleviated to some extent with the use of parameters for homologous series [36, 37] rather than single components, together with the use of predictive methods to estimate the binary interactions [38, 39]. In the case of SAFT-variants reformulations within the context of group contribution (GC) approaches [8–13] have been gained prominence in more recent

years with the aim to combine the accuracy of these sophisticated thermodynamic approaches with the predictive capabilities inherent to the GC concept. Some of these methodologies can be used to describe the properties of pure components as well as mixtures within the same group-contribution framework, whereas other employ the group contribution concept to predict only binary interaction parameters between unlike molecules [6, 7, 40]. Of particular note is also the group-contribution with association (GCA) EoS [41], which has been applied to the study of the fluid-phase behaviour of a number of associating systems, including aqueous solutions of hydrocarbons [42]. In GC-based theories, the molecular properties that describe a given compound are obtained, in accordance with the group-contribution principle, by appropriate summation of the contributions of the chemical moieties that characterize the compound of interest, and binary interactions are determined based on the corresponding functional groups. The parameters that describe the like and unlike group interactions are estimated by regression to an extensive set of experimental data for common compounds, and once determined, are used to predict the thermodynamic properties of compounds for which limited or no experimental data are available. These sophisticated thermodynamic methods can be used to describe accurately the fluid-phase behaviour of a wide-range of challenging systems, but the prediction of thermodynamic derivative properties is not always accurate [43], even for simple hydrocarbons. To achieve a more accurate representation, it has been found that the specific form of the molecular interactions, as captured by the intermolecular potential, is paramount, and that the Mie (generalized Lennard-Jonesium) potential can be used to provide an much improved model [44, 45]. The recent development of a third-order perturbation expansion for the Mie potential within the SAFT-VR Mie EoS [43] provides an accurate simultaneous representation of the fluid-phase behaviour and the second-order thermodynamic derivative properties for a variety of systems [43–47]. The perturbation theory has now been reformulated as a group-contribution equation equation of state (SAFT-γ Mie [13]) and shows promise as a generic tool for the prediction of thermodynamic properties of a wide variety of systems based on group parameters [48]. The aim of our current work is the development of models for components of special interest to the oil and gas industry within the framework of the SAFT-γ Mie EoS. We consider mixtures containing water, carbon dioxide, methanol, aromatics and alkanes.

A brief outline of the SAFT-γ Mie group contribution approach is presented next, highlighting the key features of the theory and the underlying molecular model, followed by a discussion of the systems of interest within the context of our current work, and an overview of the methodology adopted to estimate the group parameters for these systems. The performance of the theory in the description of the thermodynamic properties of selected mixtures is illustrated for a variety of property calculations and predictions and comparisons are made with other benchmark thermodynamic approaches.
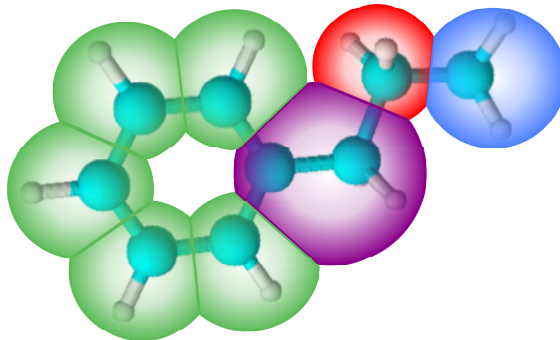
Figure 1: Pictorial representation of the heterosegment molecular model employed within the SAFT-γ Mie group contribution approach. The example shown corresponds to n-propylbenzene, where the methyl (CH_3), methanediyl (CH_2), aromatic methine (aCH), and aCCH$_2$ chemical functional groups are highlighted in blue, red, green, and purple respectively.

2. Methodology

2.1. SAFT-γ Mie models and theory

In the SAFT-γ Mie [13] EoS a model of heteronuclear chains is employed where different fused spherical segments are used to represent the distinct chemical moieties of a given molecule. An example of the heterosegment molecular model employed within the theory is shown in Figure 1 for the case of n-propylbenzene, where the constituent methyl (CH_3), methanediyl (CH_2), aromatic methine (aCH), and aCCH$_2$ chemical functional groups that characterize the molecule are highlighted.

Each compound i is defined by a set of values $\nu_{i,k}$ that denote the number of functional groups of type k in the compound. A given group k is characterized by one or more identical segments, ν_k^* and a shape factor S_k which determines the extent to which each segment contributes to the overall molecular properties. The Mie [49] pair potential model employed for the description of segment-segment interactions is a generalized form of the Lennard-Jones potential [50–54], with variable attractive and repulsive ranges. In the case of interactions between segments of the same group-type k, the Mie potential is written as

$$\Phi_{kk}^{\mathrm{Mie}}(r_{kk}) = \mathcal{C}_{kk}\varepsilon_{kk}\left[\left(\frac{\sigma_{kk}}{r_{kk}}\right)^{\lambda_{kk}^{\mathrm{r}}} - \left(\frac{\sigma_{kk}}{r_{kk}}\right)^{\lambda_{kk}^{\mathrm{a}}}\right], \tag{1}$$

where r_{kk} is the centre-centre distance between the segments, σ_{kk} is the diameter of the segments, ε_{kk} is the depth of the potential, and $\mathcal{C}_{kk}$ is a constant, function of the repulsive ($\lambda_{kk}^{\mathrm{r}}$) and attractive ($\lambda_{kk}^{\mathrm{a}}$) exponents of the potential defined as

$$\mathcal{C}_{kk} = \frac{\lambda_{kk}^{\mathrm{r}}}{\lambda_{kk}^{\mathrm{r}} - \lambda_{kk}^{\mathrm{a}}}\left(\frac{\lambda_{kk}^{\mathrm{r}}}{\lambda_{kk}^{\mathrm{a}}}\right)^{\frac{\lambda_{kk}^{\mathrm{a}}}{\lambda_{kk}^{\mathrm{r}} - \lambda_{kk}^{\mathrm{a}}}}, \tag{2}$$

which ensures that the minimum of the potential is at ε_{kk}.

5

The group interactions are thus characterized by the diameter of each segment σ_{kk}, the potential well-depth ε_{kk}, and the repulsive and attractive ranges of the interaction potential $\lambda_{kk}^{\mathrm{r}}$ and $\lambda_{kk}^{\mathrm{a}}$, respectively. Association between groupd where appropriate is treated by the addition of square-well short-ranged bonding sites on the group segments, as commonly employed within SAFT-type approaches. Together with the number of different site types characterizing the association of a group $N_{\mathrm{ST},k}$, and the number of sites of a given a type $n_{k,a}$ which are typically chosen *a priori*, the energy $\varepsilon_{kk,ab}^{\mathrm{HB}}$ of the association interaction between sites of types a and b, and the corresponding bonding volume $K_{kk,ab}$ which describes the geometric component of this association interaction are required for the complete description of associating interactions.

The interaction between unlike groups k and l is characterized by an unlike segment diameter σ_{kl} defined as

$$\sigma_{kl} = \frac{\sigma_{kk} + \sigma_{ll}}{2} \ , \tag{3}$$

the unlike Barker-Henderson effective hard-sphere diameter as

$$d_{kl} = \frac{d_{kk} + d_{ll}}{2} \ , \tag{4}$$

the unlike dispersion energy (obtained using a modified geometric mean that takes into account the size asymmetry of the groups as [39])

$$\varepsilon_{kl} = \frac{\sqrt{\sigma_{kk}^3 \sigma_{ll}^3}}{\sigma_{kl}^3} \sqrt{\varepsilon_{kk} \varepsilon_{ll}} \ , \tag{5}$$

and the unlike repulsive and attractive exponents of the Mie potentials as

$$\lambda_{kl} = 3 + \sqrt{(\lambda_{kk} - 3)(\lambda_{ll} - 3)} \ . \tag{6}$$

These combing rules are determined from a geometric mean of the van der Waals integrated energy of the respective Sutherland potentials [13, 43]. The unlike association parameters are defined as

$$\varepsilon_{kl,ab}^{\mathrm{HB}} = \sqrt{\varepsilon_{kk,aa}^{\mathrm{HB}} \varepsilon_{ll,bb}^{\mathrm{HB}}} \ , \tag{7}$$

and

$$K_{kl,ab} = \left(\frac{\sqrt[3]{K_{kk,aa}} + \sqrt[3]{K_{ll,bb}}}{2} \right)^3 \ . \tag{8}$$

The values obtained through these combining rules are often refined by regression to experimental data to capture more accurately the physics features of the specific interactions. In our current work, as in other works with the SAFT-γ Mie EoS, the unlike segment and hard-sphere diameters as well as the unlike attractive exponent are always given by equations (3), (4), and (6).

Once the models for the chemical functional groups characterizing the system have been established, the Helmholtz free energy can be determined following the expressions presented in previous work [13, 48], with the association contribution detailed in Ref. [46]. Other thermodynamic properties can be obtained from the free energy from the standard thermodynamic relations.

Table 1: Summary of the SAFT-γ Mie functional groups and unlike interactions required for the modelling of the mixtures of interest in our current work. The stars indicate the like and unlike parameters required for the modelling of the systems of interest developed here, while the literature references indicate interactions developed previously [13, 46, 48].

	CH$_3$	CH$_2$	aCH	aCCH$_3$	aCCH$_2$	CH$_4$	H$_2$O	CH$_3$OH	CO$_2$
CH$_3$	[13]								
CH$_2$	[13]	[13]							
aCH	★	★	★						
aCCH$_3$	-	-	★	★					
aCCH$_2$	★	★	★	-	★				
CH$_4$	-	-	-	-	-	★			
H$_2$O	★	★	-	-	-	★	[46]		
CH$_3$OH	★	★	-	-	-	★	★	★	
CO$_2$	★	★	-	-	-	★	★	★	★

2.2. Systems of interest and definition of groups

The aim of the work presented in our current study is to investigate the suitability of the SAFT-γ Mie GC approach to model mixtures of components of relevance to the oil and gas industry. These include mixtures of carbon dioxide, water, methanol, methane, linear alkanes (ethane to n-decane), and aromatic hydrocarbons (benzene, toluene, and alkylbenzenes). Of the compounds listed, carbon dioxide, water, methanol, and methane are modelled as molecular groups, e.g., the CO$_2$ group for carbon dioxide, the CH$_3$OH group for methanol, etc. For the linear alkanes the parameters readily available for the methyl (CH$_3$) and methanediyl (CH$_2$) groups from previous work [13, 48] are employed. The aromatic hydrocarbons are modelled by developing new aCH, aCCH$_2$, and aCCH$_3$ functional groups in our current work. Benzene is modelled with six equivalent aCH groups, toluene as 5×aCH and 1×aCCH$_3$ groups, and the n-alkylbenzenes as 5×aCH, 1×aCCH$_2$ and the appropriate number of CH$_3$ and CH$_2$ groups of the alkyl chain. The functional groups that are required to fully characterize the mixtures of interest are summarized in Table 1, where the functional groups and the unlike interactions considered are highlighted. (As shown in Table 1, not all unlike interactions between the listed functional groups are required for the characterization of the mixtures of interest.) The values of some of the parameters have already been collected in an earlier paper [48]; here we provide details of the parameter-estimation procedure and performance of the models.

2.3. Parameter estimation

Within the framework of the SAFT-γ Mie GC approach all functional groups k (molecular or not) are characterized by the following set of parameters: the number of spherical segments ν_k^*, the shape factor S_k,

the segment diameter σ_{kk}, the dispersive energy ε_{kk}, and the repulsive and attractive ranges of the potential $\lambda_{kk}^{\mathrm{r}}$ and $\lambda_{kk}^{\mathrm{a}}$, respectively. For associating groups, such as the H_2O and CH_3OH molecules considered here, additional parameters are required, namely, the energy $\varepsilon_{kkab}^{\mathrm{HB}}$ and extent K_{kkab} of the association interactions, the number of sites $n_{k,a}$ of each type a for each group, together with the total number of site types $N_{\mathrm{ST},k}$. In practice ν_k^*, $N_{\mathrm{ST},k}$, and $n_{k,a}$ are assigned fixed values based on the chemical nature of each group or, in some cases, with a trial-and-error approach. Of the parameters that describe the unlike dispersion interactions between functional groups, only the unlike dispersion energy ε_{kl}, and in some cases the value of the unlike repulsive exponent $\lambda_{kl}^{\mathrm{r}}$, are adjusted to reproduce the experimental pure component and mixture data more accurately. For the description of associating interactions between different functional groups the value of the unlike energy of association $\varepsilon_{klab}^{\mathrm{HB}}$, and extent of association K_{klab} are also treated as adjustable parameters. All other unlike interaction parameters are determined by means of appropriate combining rules as discussed in section 2.1 and in Refs.[13, 46, 48].

Either pure component data or mixture data are employed in the characterization of group parameters. In the case of molecular groups, such as H_2O, CO_2, CH_4, and CH_3OH, the model parameters are estimated from the pure-component vapour-liquid equilibrium (VLE) data for each substance. Vapour-pressure P_{vap}, and saturated-liquid density ρ_{sat} data are typically employed. Additional experimental single-phase liquid densities, or even second-order thermodynamic derivative properties, such as the speed of sound or heat capacities, can sometimes be useful in order to improve the physical significance of the molecular parameters; single-phase data are not used in our current work. The objective function used in the estimation of molecular group parameters is of the following form:

$$
\min_{\boldsymbol{\Omega}} f_{\mathrm{obj}} = w_P \sum_{m=1}^{N_{P_{\mathrm{vap}}}} \left[\frac{P_{\mathrm{vap}}^{\exp}(T_m) - P_{\mathrm{vap}}^{\mathrm{calc}}(T_m; \boldsymbol{\Omega})}{P_{\mathrm{vap}}^{\exp}(T_m)} \right]^2 \\
+ w_\rho \sum_{n=1}^{N_{\rho_{\mathrm{sat}}}} \left[\frac{\rho_{\mathrm{sat}}^{\exp}(T_n) - \rho_{\mathrm{sat}}^{\mathrm{calc}}(T_n; \boldsymbol{\Omega})}{\rho_{\mathrm{sat}}^{\exp}(T_n)} \right]^2 ,
\tag{9}
$$

where $\boldsymbol{\Omega}$ represents the vector of estimated parameters, and w_P and w_ρ are weighting factors that can be adjusted according to desired level of accuracy for each property; in our current work equal weights $w_P = w_\rho = 1$ are employed. The summations in equation (9) are over the number of experimental points $N_{P_{\mathrm{vap}}}$ for the vapour pressure, and $N_{\rho_{\mathrm{sat}}}$ for the saturated-liquid density considered in the parameter estimation. The minimizations are performed using the numerical solvers provided by the commercial software package gPROMS$^{\copyright}$ [55].

In the case of other (non-molecular) groups the determination of the parameters describing the groups of interest is carried out using experimental data for several molecules comprising the corresponding groups, such as benzene and the n-alkylbenzenes for the determination of the aCH and aCCH$_2$ group parameters. In order to enhance the physical significance of the parameters obtained, mixture data (fluid-phase equilibria

or excess properties of mixing) can also be included in the estimation procedure; in our current work some excess enthalpy and volumetric data are included, leading to the following objective function:

$$
\begin{aligned}
\min_{\boldsymbol{\Omega}} f_{\text{obj}} = & \; w_P \sum_{i=1}^{N_C} \sum_{m=1}^{N_{P_{\text{vap}}}} \left[\frac{P_{\text{vap},i}^{\text{exp}}(T_m) - P_{\text{vap},i}^{\text{calc}}(T_m; \boldsymbol{\Omega})}{P_{\text{vap},i}^{\text{exp}}(T_m)} \right]^2 \\
& + w_\rho \sum_{i=1}^{N_C} \sum_{n=1}^{N_{\rho_{\text{sat}}}} \left[\frac{\rho_{\text{sat},i}^{\text{exp}}(T_n) - \rho_{\text{sat},i}^{\text{calc}}(T_n; \boldsymbol{\Omega})}{\rho_{\text{sat},i}^{\text{exp}}(T_n)} \right]^2 \\
& + w_h \sum_{j=1}^{N_{h^E}} \left[\frac{h^{E,\text{exp}}(T_j; P_j; x_j) - h^{E,\text{calc}}(T_j; P_j; x_j; \boldsymbol{\Omega})}{h^{E,\text{exp}}(T_j; P_j; x_j)} \right]^2 \\
& + w_v \sum_{j=1}^{N_{v^E}} \left[\frac{v^{E,\text{exp}}(T_j; P_j; x_j) - v^{E,\text{calc}}(T_j; P_j; x_j; \boldsymbol{\Omega})}{v^{E,\text{exp}}(T_j; P_j; x_j)} \right]^2,
\end{aligned}
\tag{10}
$$

where the first two sums are over the N_C pure components i included in the estimation, while the last two terms run over the number N_{h^E} of experimental excess enthalpy points, and N_{v^E} of excess volume data points considered; in addition the weights are taken as equal with $w_P = w_\rho = w_h = w_v = 1$. The n-alkylbenzenes also comprise the CH_3 and CH_2 groups, which have been characterized in previous work [13]; the estimation group-group parameters using these data provides additional values for the unlike interactions between the aCH-CH_3 , aCH-CH_2, aCCH_2-CH_3 and aCCH_2-CH_2 groups. This is a unique characteristic of heterosegment SAFT approaches that greatly enhances their predictive capability, as has been demonstrated for the case of the n-alkanes with the SAFT-γ Mie GC approach [13, 48], as well as with other approaches [9–11, 56, 57]. Our new parameters hence enables the description of mixtures of benzene, n-alkylbenzenes and alkanes without further parameter estimation.

In the case of mixtures involving molecular groups experimental binary mixture data needs to be considered to estimate the unlike interaction parameters. Here we use fluid-phase equilibrium data and the corresponding objective function is given by

$$
\begin{aligned}
\min_{\boldsymbol{\Omega}} f_{\text{obj}} = & \; \frac{w_x}{N_x} \sum_{m=1}^{N_x} \left[x^{\text{exp}}(T_m, P_m) - x^{\text{calc}}(T_m, P_m; \boldsymbol{\Omega}) \right]^2 \\
& + \frac{w_y}{N_y} \sum_{n=1}^{N_y} \left[y^{\text{exp}}(T_n, P_n) - y^{\text{calc}}(T_n, P_n; \boldsymbol{\Omega}) \right]^2,
\end{aligned}
\tag{11}
$$

and expresses the sum of the square of the residuals between the experimental (exp) and calculated (calc) values of the liquid $x(T, P)$ and vapour $y(T, P)$ compositions of a given mixture at specified values of the pressure and temperature over all experimental points (N_x for the liquid and N_y for the vapour phase). The desired level of accuracy in each of the phases can be tuned by adjusting the weighting factors for the liquid w_x or the vapour w_y phases. As the objective function of equation (11) is expressed in terms of mole fractions, which are constrained to be between zero and one, the use of an absolute error is considered more appropriate. In our work the calculation of the fluid-phase behaviour is undertaken by means of a reliable

P-T algorithm [58] and a multi-start gradient-based algorithm is used for parameter estimation.

The metric used in our work to quantify the quality of the theoretical description of the experimental data in the case of pure compounds is the percentage average absolute deviation (%AAD), defined for a given property R as

$$\%\text{AAD } R = \frac{1}{N_R} \sum_{i=1}^{N_R} \left| \frac{R_i^{\text{exp.}} - R_i^{\text{calc.}}}{R_i^{\text{exp.}}} \right| \times 100 \ , \tag{12}$$

where N_R is the number of data points of property R, and $R_i^{\text{calc.}}$ and $R_i^{\text{exp.}}$ are the calculated and experimental values for the same property, respectively, at the conditions of the ith experimental point. For the case of binary mixtures absolute errors in composition are reported, defined as

$$\Delta z = \frac{1}{N_z} \sum_{i=1}^{N_z} \left| z_i^{\text{exp.}} - z_i^{\text{calc.}} \right| \times 100 \ , \tag{13}$$

where N_z is the number of data points, and $z_i^{\text{calc.}}$ and $z_i^{\text{exp.}}$ are the calculated and experimental values for the composition, respectively, at the conditions of the ith experimental point.

All SAFT-γ Mie group parameters used in our current work are reported in Tables 2 to 4. Some of these parameters have been reported previously [13, 46, 48] and this is indicated in the tables. In addition, further details related to the development of the parameters that was not provided in earlier work is now given for completeness together with the description of the development of new parameters carried out in our current work.

3. Results and discussion

We consider now the characterization of each of the SAFT-γ Mie group-group interactions needed to treat the fluids of interest. We present first the development of the proposed group parameters from pure component data and their adequacy, followed by the study of binary mixtures and the estimation of unlike interaction parameters; the predictive capability of the SAFT-γ Mie GC approach in describing ternary mixtures is then investigated.

3.1. Pure components

The parameters characterising the molecular groups of methane (CH_4), carbon dioxide (CO_2), water (H_2O), and methanol (CH_3OH), and the functional groups for the modelling of the family of *n*-alkylbenzenes (aCH and aCCH$_2$) and toluene (aCCH$_3$), are developed based on pure-component vapour-liquid equilibrium (VLE) experimental data only (i.e., no single-phase data are used). The temperature range of the data included in the estimation of group parameters is from 30 to 90% of the experimental critical temperature for each compound.

Table 2: Like group parameters for use within the SAFT-γ Mie group-contribution approach: ν_k^*, S_k, and σ_{kk} are the number of segments constituting group k, the shape factor, and the segment diameter of group k, respectively; $\lambda_{kk}^{\mathrm{r}}$ and $\lambda_{kk}^{\mathrm{a}}$ are the repulsive and attractive exponents, and ε_{kk} is the dispersion energy of the Mie potential characterizing the interaction between two k groups and k_{B} is the Boltzmann constant; $N_{\mathrm{ST},k}$ represents the number of association site types on group k, with $n_{k,H}$ and $n_{k,e}$ denoting the number of association sites of type H and e respectively.

k	Group k	ν_k^*	S_k	$\lambda_{kk}^{\mathrm{r}}$	$\lambda_{kk}^{\mathrm{a}}$	σ_{kk} / Å	$(\varepsilon_{kk}/k_{\mathrm{B}})$ / K	$N_{\mathrm{ST},k}$	$n_{k,H}$	$n_{k,e}$	Ref.
1	CH_3	1	0.57255	15.050	6.0000	4.0773	256.77	–	–	–	[13]
2	CH_2	1	0.22932	19.871	6.0000	4.8801	473.39	–	–	–	[13]
3	aCH	1	0.32184	14.756	6.0000	4.0578	371.53	–	–	–	[48]
4	$aCCH_3$	1	0.31655	23.627	6.0000	5.4874	651.41	–	–	–	current work
5	$aCCH_2$	1	0.20859	8.5433	6.0000	5.2648	591.56	–	–	–	[48]
6	CH_4	1	1.00000	12.504	6.0000	3.7370	152.58	–	–	–	current work
7	H_2O	1	1.00000	17.020	6.0000	3.0063	266.68	2	2	2	[46]
8	CH_3OH	2	0.83517	19.235	6.0000	3.2462	307.69	2	1	2	[48]
9	CO_2	2	0.84680	26.408	5.0550	3.0500	207.89	1	1	0	current work

Methane is modelled by means of the molecular group CH_4, consisting of a single spherical segment (i.e., with the shape factor fixed to one) and the attractive Mie potential exponent fixed to the London value of 6. The remaining parameters are estimated using pure methane vapour pressure and saturated-liquid density data [59]. The resulting model provides a very good description of the VLE of methane, as illustrated in Figure 2.

Carbon dioxide is modelled by means of the molecular group CO_2, formed from two fused Mie segments. An unlike induced association-site of type H is also included in order to model the phase behaviour of carbon dioxide + water mixtures, c.f. section 3.2; this site is inactive in the absence of water [60], i.e., $\varepsilon_{CO_2CO_2,HH}^{\mathrm{HB}} = 0$. This type of association scheme for aqueous mixtures of CO_2 has been proposed previously and employed in other work [61–63]). The CO_2-CO_2 interaction group parameters are estimated using pure carbon dioxide vapour pressure and saturated-liquid density data [59]. The description of the VLE of pure carbon dioxide obtained with the estimated parameters is excellent, as can be seen from Figure 2. As has been shown in previous work [13, 46, 48, 60], one of the strengths of the SAFT-γ Mie (and the underlying SAFT-VR Mie [43]) approach is the accuracy of the predictions of single-phase and second-derivative properties (density, heat capacity, speed of sound) from parameters estimated using VLE data. The SAFT-γ Mie predictions for single-phase density and isobaric heat capacity of carbon dioxide are provided in Figure 3 and compared to corresponding experimental data; the excellent agreement of the predictions with the measured data is apparent.

The H_2O molecular group used to model water comprises a single Mie segment with four association

Table 3: Group dispersion interaction energies ε_{kl} and repulsive exponent $\lambda^{\mathrm{r}}_{kl}$ for use within the SAFT-γ Mie group-contribution approach. In all cases the unlike group diameters σ_{kl} and d_{kl} as well as the unlike attractive exponent of the Mie potential $\lambda^{\mathrm{a}}_{kl}$ are obtained from the combining rules defined in equations (3), (4), and (6), respectively. CR indicates that the unlike repulsive exponent $\lambda^{\mathrm{r}}_{kl}$ is obtained from Equation (6).

k	l	Group k	Group l	$(\varepsilon_{kl}/k_{\mathrm{B}})$ / K	$\lambda^{\mathrm{r}}_{kl}$	Ref.
1	1	CH_3	CH_3	256.77	15.050	[13]
1	2	CH_3	CH_2	350.77	CR	[13]
1	3	CH_3	aCH	305.81	CR	[48]
1	5	CH_3	$aCCH_2$	396.91	CR	[48]
1	7	CH_3	H_2O	274.80	CR	[48]
1	8	CH_3	CH_3OH	275.76	15.537	[48]
1	9	CH_3	CO_2	205.70	CR	current work
2	2	CH_2	CH_2	473.39	19.871	[13]
2	3	CH_2	aCH	415.64	CR	[48]
2	5	CH_2	$aCCH_2$	454.16	CR	[48]
2	7	CH_2	H_2O	284.53	CR	[48]
2	8	CH_2	CH_3OH	341.41	17.050	[48]
2	9	CH_2	CO_2	276.45	CR	current work
3	3	aCH	aCH	371.53	14.756	[48]
3	4	aCH	$aCCH_3$	471.23	CR	current work
3	5	aCH	$aCCH_2$	416.69	CR	[48]
4	4	$aCCH_3$	$aCCH_3$	654.41	23.627	current work
5	5	$aCCH_2$	$aCCH_2$	591.56	8.5433	[48]
6	6	CH_4	CH_4	152.58	12.504	current work
6	7	CH_4	H_2O	175.41	CR	current work
6	8	CH_4	CH_3OH	233.21	CR	current work
6	9	CH_4	CO_2	144.72	11.950	current work
7	7	H_2O	H_2O	266.68	17.050	[46]
7	8	H_2O	CH_3OH	278.45	CR	[48]
7	9	H_2O	CO_2	226.38	CR	current work
8	8	CH_3OH	CH_3OH	307.69	19.235	[48]
8	9	CH_3OH	CO_2	157.83	8.3462	current work
9	9	CO_2	CO_2	207.89	26.408	current work

Table 4: Group association energies $\varepsilon_{kl,ab}^{\mathrm{HB}}$ and bonding volume parameters $K_{kl,ab}$ for use within the SAFT-γ Mie group-contribution approach. For groups with two site types, the interactions are symmetrical, e.g., $\varepsilon_{kl,ab}^{\mathrm{HB}} = \varepsilon_{kl,ba}^{\mathrm{HB}}$. Other interactions not reported here are set to zero, e.g., $\varepsilon_{\mathrm{CO_2CO_2},HH}^{\mathrm{HB}} = 0$.

k	l	Group k	Site a of group k	Group l	Site b of group l	$(\varepsilon_{kl,ab}^{\mathrm{HB}}/k_{\mathrm{B}})$ / K	$K_{kl,ab}$ / Å^3
7	7	H_2O	H	H_2O	e	1985.4	101.69
7	8	H_2O	H	CH_3OH	e	1993.5	104.11
7	8	H_2O	e	CH_3OH	H	1993.5	104.11
7	9	H_2O	e	CO_2	H	1398.1	91.419
8	8	CH_3OH	H	CH_3OH	e	2062.1	106.57
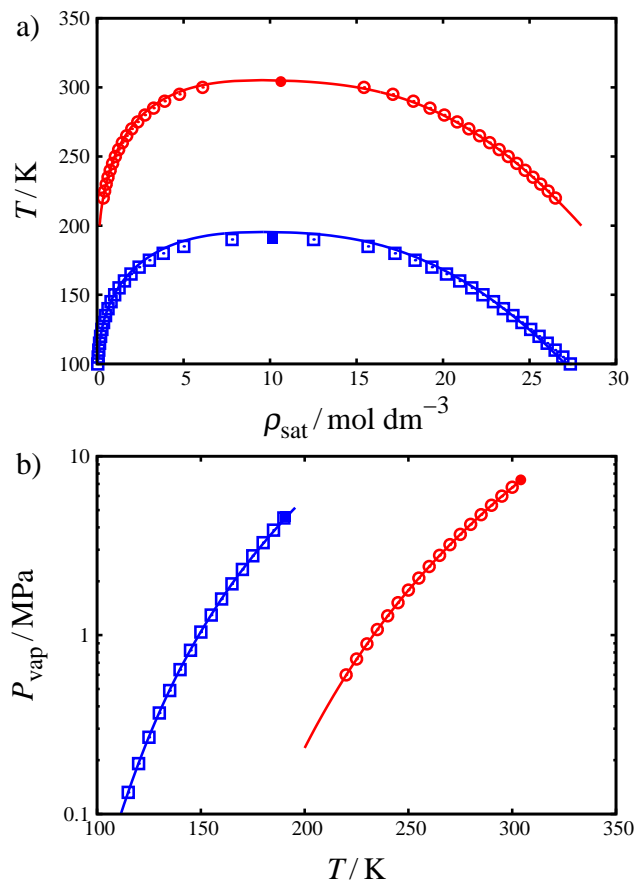
Figure 2: Vapour-liquid equilibria of pure methane and carbon dioxide. The symbols represent the experimental data [59] for methane (squares) and carbon dioxide (circles) and the continuous curves the description with the SAFT-γ Mie approach [13]: (a) saturated densities, and (b) vapour pressures. The filled symbols correspond to the experimental critical points.
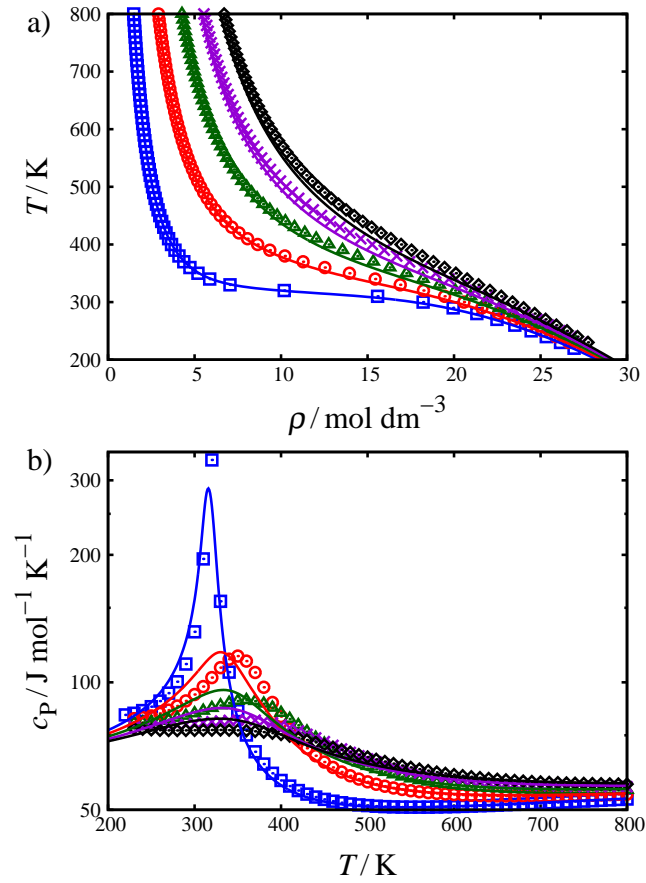
Figure 3: Single-phase properties of pure carbon dioxide. The symbols represent the experimental data [59] at pressures of $P = 10$ MPa (squares), $P = 20$ MPa (circles), $P = 30$ MPa (triangles), $P = 40$ MPa (crosses), and $P = 50$ MPa (diamonds) and the continuous curves the predictions with the SAFT-γ Mie approach [13]: (a) single-phase densities, (b) isobaric heat capacities.
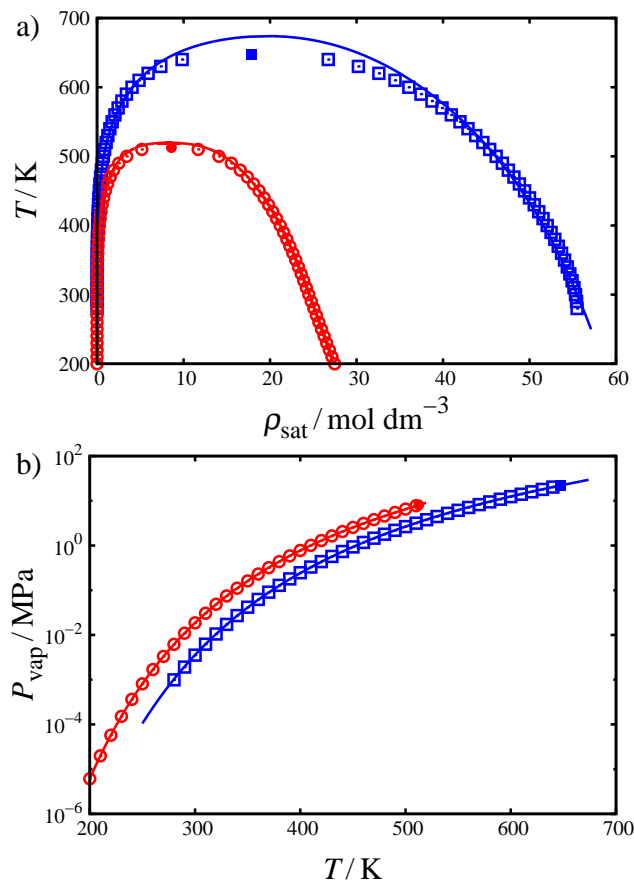
Figure 4: Vapour-liquid equilibria of pure methanol and water. The symbols represent the experimental data [59] for methanol (circles) and water (squares) and the continuous curves the description with the SAFT-γ Mie approach [13]: (a) saturated densities, (b) vapour pressures. The filled symbols correspond to the experimental critical points.

sites (two sites of type e and two sites of type H). The parameters were presented in Ref. [46], and were determined using experimental vapour pressure and saturated-liquid density data [59]. The description of the VLE obtained with this model is illustrated in Figure 4.

Methanol is modelled with the CH_3OH molecular group comprising two fused Mie segments and three association sites (two sites of type e and one site of type H). The parameters are estimated using experimental methanol VLE data [59], as before. The phase behaviour of methanol as described by the SAFT-γ Mie approach [13] and experimental data are shown in Figure 4.

The aromatic aCH, aCCH$_2$, and aCCH$_3$ groups used to model benzene, toluene, and the n-alkylbenzenes are represented as single Mie segments. The parameters describing the aCH and aCCH$_2$ groups as well as the aCH-aCCH$_2$, aCH-CH$_3$, aCH-CH$_2$, aCCH$_2$-CH$_3$, and aCCH$_2$-CH$_2$ unlike group interactions are estimated using experimental VLE data for pure benzene, and alkylbenzenes from n-ethylbenzene to n-decylbenzene [64–84], as well as excess enthalpies for the benzene + n-propylbenzene binary mixture at

15

Table 5: Percentage average absolute deviations (%AAD) for the vapour pressures $P_{\mathrm{vap}}(T)$ and the saturated-liquid densities $\rho_{\mathrm{sat}}(T)$ obtained with the SAFT-γ Mie group-contribution approach [13] (where n is the number of data points) for the pure components of interest in our current work.

Compound	T range / K	n	%AAD $P_{\mathrm{vap}}(T)$	Ref.	T range / K	n	%AAD $\rho_{\mathrm{sat}}(T)$	Ref.
Methane	95–190	20	0.70	[59]	95–190	20	2.16	[59]
Carbon dioxide	220–300	17	0.07	[59]	220–300	17	0.41	[59]
Benzene	280– 540	53	2.52	[59]	280– 540	53	1.04	[59]
Toluene	220–530	32	0.55	[59]	220–530	32	0.35	[59]
Water	280–640	37	1.15	[59]	280–640	37	1.95	[59]
Methanol	180–510	34	0.43	[59]	180–510	34	0.72	[59]
n-ethylbenzene	424–555	29	1.10	[65]	183–490	38	0.49	[70, 82]
n-propylbenzene	283–433	25	1.77	[69, 79]	223–543	20	0.43	[68, 75, 84]
n-butylbenzene	313–523	43	0.99	[73, 76, 81, 82]	223–583	22	0.44	[66, 68, 75, 78, 81, 82]
n-pentylbenzene	293–477	18	2.63	[72, 79, 83]	233-633	14	1.46	[74, 75]
n-hexylbenzene	264–463	27	1.57	[77]	253–613	53	0.37	[71, 75]
n-heptylbenzene	309–513	20	5.30	[72, 83]	281–368	11	0.25	[72, 74]
n-octylbenzene	293–463	25	5.24	[64, 73]	243–648	12	1.00	[75]
n-nonylbenzene	332–466	29	3.30	[64, 77, 80]	282–368	9	0.14	[72]
n-decylbenzene	343–571	25	1.82	[67, 73, 83]	273–678	11	1.35	[75]

ambient conditions ($T = 298.15$ K, $P = 1$ atm) [85]. The aCCH$_3$ like parameters and the aCH-aCCH$_3$ unlike group interaction are estimated using vapour pressure and saturated-liquid density data [59] of pure toluene, as well as excess enthalpies and volumes for the toluene + benzene binary mixture at ambient conditions ($T = 298.15$ K, $P = 1$ atm) [86, 87]. The models obtained, summarized in Tables 2 to 4 are found to provide a good representation of the vapour pressures and saturated-liquid densities of the pure components, as can be seen from the values of the %AADs presented in Table 5.

3.2. Binary Mixtures

In this section the characterization of the remaining unlike group interaction parameters involving at least one molecular group is discussed and the performance of the SAFT-γ Mie approach in describing the properties of binary mixtures containing the compounds of interest is investigated. We first consider mixtures containing alkanes of different chain length and one other component chosen from carbon dioxide, methanol, and water, illustrating the increasing non-ideality of the fluid-phase behaviour exhibited by these systems as one of the components becomes more polar. Mixtures not containing alkanes, namely, water + carbon dioxide and water + methanol, are then considered.

An accurate description of the properties of mixtures containing n-alkanes and carbon dioxide is important in the oil and gas industry as methane and the alkanes are prevalent components of crude oil and natural

gas, while carbon dioxide is ubiquitous, either as naturally occurring in the reservoir fluids or injected in the context of enhanced oil recovery or carbon storage. It is also of interest to note that the type of fluid-phase behaviour exhibited by binary mixtures of carbon dioxide and n-alkanes changes with the chain length of the alkane [88, 89].

As mentioned previously, methane is represented as a single Mie sphere and carbon dioxide as two fused Mie segments in SAFT-γ Mie approach. Methane and carbon dioxide are both modelled with molecular groups so that is not possible to determine their unlike interactions using pure component data; instead these are estimated using the fluid-phase equilibria experimental data for the carbon dioxide + methane mixture. The unlike dispersion energy ε_{kl}, and repulsive Mie exponent $\lambda_{kl}^{\mathrm{r}}$ are determined using isothermal VLE data at 240 and 270 K [90]. The resulting interaction parameter values are presented in Table 3. In Figure 5(a) the SAFT-γ Mie description of the phase behaviour is compared to the experimental data for the temperatures considered in the parameter estimation [90] and for two other isotherms [91] that are obtained predicively. The fluid-phase behaviour obtained using the PPR78 equation of state [25] is also included in the figure for comparison. The PPR78 model is considered one of the most accurate predictive cubic EoSs, often used in the modelling of these substances within the oil and gas industry. The comparison with SAFT-γ Mie EoS presented in Figure 5 provides a validation of the accuracy of our group-contribution methododology.

The n-alkanes are modelled in SAFT-γ Mie with the appropriate number of CH_3 and CH_2 groups, so that the complete series of carbon dioxide + n-alkane binary mixtures can be treated from the determination of just two unlike interactions between the CH_3-CO_2 and CH_2-CO_2 groups. In this work only the unlike dispersion energies ε_{kl} are estimated. Experimental VLE data for carbon dioxide + n-decane at 344.23 and 377.59 K [92], as well as carbon dioxide + n-pentane at 344.15 and 377.59 K [93] are used to characterize the unlike dispersion energies. The resulting interaction-parameter values are displayed in Table 3. Once the group parameters have been determined the fluid-phase behaviour of different carbon dioxide + n-alkane mixtures can be predicted, as illustrated in Figures 5(b) and (c) for carbon dioxide mixtures containing n-propane and n-decane, respectively. In the figures the predictions of the SAFT-γ Mie approach are compared with experimental data [92, 94] and with calculations carried out using the PPR78 EoS [25]. The very good descriptions obtained with SAFT-γ Mie underline the transferability of the SAFT-γ Mie models to conditions (in the case of n-decane) and compounds (in the case of n-propane) removed from the parameter estimation procedure.

The versatility of the SAFT-γ Mie approach is further illustrated in Figure 6 where the excess properties of mixing of two binary mixtures predicted from SAFT-γ Mie EoS are compared with the corresponding experimental data [95, 96]. The excess enthalpy of mixing for carbon dioxide + n-pentane at different temperatures and pressures is presented in Figure 6(a) and the excess volume of mixing of carbon dioxide + n-hexane at different temperatures and pressures in Figure 6(b). The effect of a change in temperature

or pressure is captured well with the approach, leading to a near-quantitative description of the excess properties considered.

Methanol is widely used in the oil and gas industry as a thermodynamic inhibitor to prevent the formation of clathrate hydrates [16]. As such, an accurate description of the properties of its mixtures with alkanes and water is essential. The fluid-phase behaviour of methane + methanol [98, 99] is of type III based on the classification of van Konynenburg and Scott [100], with entensive regions of liquid-liquid demixing. Mixtures of longer alkanes with methanol present different types of fluid-phase behaviour. The binary mixture of ethane + methanol also exhibits type III behaviour, while n-propane + methanol and mixtures involving longer n-alkanes and methanol exhibit type II behaviour [99].

A treatment of the entire series of methanol + alkane binary mixtures from methane to long alkanes requires the determination of the CH_4-CH_3OH unlike interaction for the case of the methane + methanol mixture, as well as those of the CH_3-CH_3OH and CH_2-CH_3OH unlike interactions for the other n-alkane + methanol mixtures. The CH_4-CH_3OH unlike interaction parameters (unlike dispersion energy, ε_{kl}, and repulsive exponent, λ_{kl}^{r}) are estimated using experimental phase equilibrium data at 290 and 330 K [101], and the corresponding values are reported in Table 3. Once the parameters have been determined, they are validated with predictions of two additional isotherms at 273.15 and 310 K. The results are compared to experimental data [101] in Figure 7. The SAFT-γ Mie approach provides an excellent description of the composition of the two phases, as evidenced by Figures 7(b) and (c). A particular feature of this system is the trend of solubility of methane in the methanol-rich phase: at pressures below 30 MPa the solubility decreases with increasing temperature, whereas at higher pressures the opposite is observed. This feature is captured very well with the SAFT-γ Mie EoS, as is apparent from the figure.

The CH_3-CH_3OH and CH_2-CH_3OH unlike interaction parameters (unlike dispersion energy ε_{kl} and repulsive exponent λ_{kl}^{r}) are estimated using experimental n-hexane + methanol isobaric phase equilibrium data at 0.101 MPa [102, 103]. The values of the group parameters are presented in Table 3. These parameters are then used to predict the fluid-phase behaviour of the mixtures of methanol with two shorter n-alkanes (ethane and n-butane). A comparison of the SAFT-γ Mie description with the experimental data for these mixtures as well as the predictions for n-hexane + methanol [102–105] is made in Figure 8. The description provided by SAFT-γ Mie in the case of n-hexane + methanol is very good, both for the VLE and LLE regions. The predictive capabilities of the approach is confirmed by the quality of the predictions in the case of the ethane + methanol and n-butane + methanol systems, with the VLE, LLE, and three-phase VLLE well described.

Mixtures of alkanes with water are notoriously difficult to model due to the extreme liquid-liquid demixing (type III phase behaviour) encountered in these systems, with solubilities that differ by orders of magnitude between the two coexisting phases. In order to model the methane + water system, the CH_4-H_2O unlike interaction needs to be determined. The unlike dispersion energy (ε_{kl}) between the two molecular groups
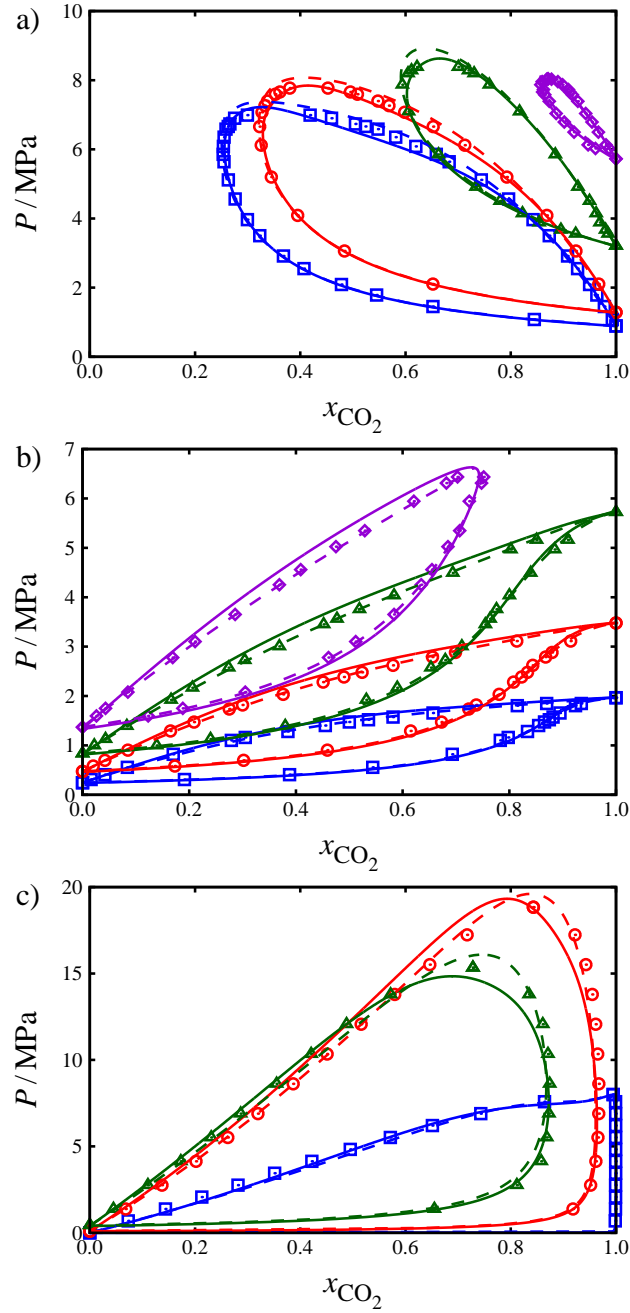
Figure 5: Isothermal pressure-mole fraction (P-x) vapour-liquid equilibria of selected binary mixtures of carbon dioxide + n-alkanes. The symbols represent the experimental data, the continuous curves the description with the SAFT-γ Mie approach [13] and the dashed curves the description with the PPR78 equation of state [25]: (a) phase diagram of carbon dioxide + methane at temperatures of $T = 230$ K [91] (squares), $T = 240$ K [90] (circles), $T = 270$ K [91] (triangles), and $T = 293$ K [97] (diamonds); (b) fluid-phase diagram of carbon dioxide + n-propane [94] at temperatures of $T = 253.15$ K (squares), $T = 273.15$ K (circles), $T = 293.15$ K (triangles), and $T = 313.15$ K (diamonds); (c) phase diagram of carbon dioxide + n-decane [92] at temperatures of $T = 310.93$ K (squares), $T = 444.26$ K (circles), and $T = 510.93$ K (triangles).

19
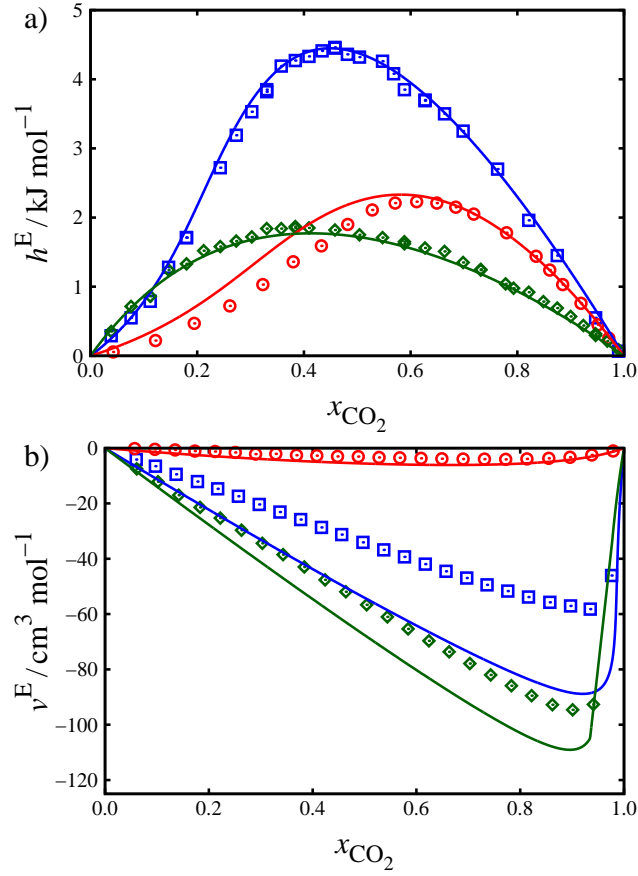
Figure 6: Isothermal-isobaric excess properties of mixing for carbon dioxide + n-alkane binary mixtures. The symbols represent the experimental data and the continuous curves the predictions with the SAFT-γ Mie approach [13]: (a) excess molar enthalpy of mixing for carbon dioxide + n-pentane [95] at temperatures and pressures of $T = 470.15$ K - $P = 7.58$ MPa (squares), $T = 470.15$ K - $P = 12.45$ MPa (circles), and $T = 573.15$ K - $P = 7.58$ MPa (diamonds); (b) excess molar volume of mixing for carbon dioxide + n-hexane [96] at temperatures and pressures of $T = 308.15$ K - $P = 7.5$ MPa (squares), $T = 308.15$ K - $P = 10.5$ MPa (circles), and $T = 313.15$ K - $P = 7.5$ MPa (diamonds).
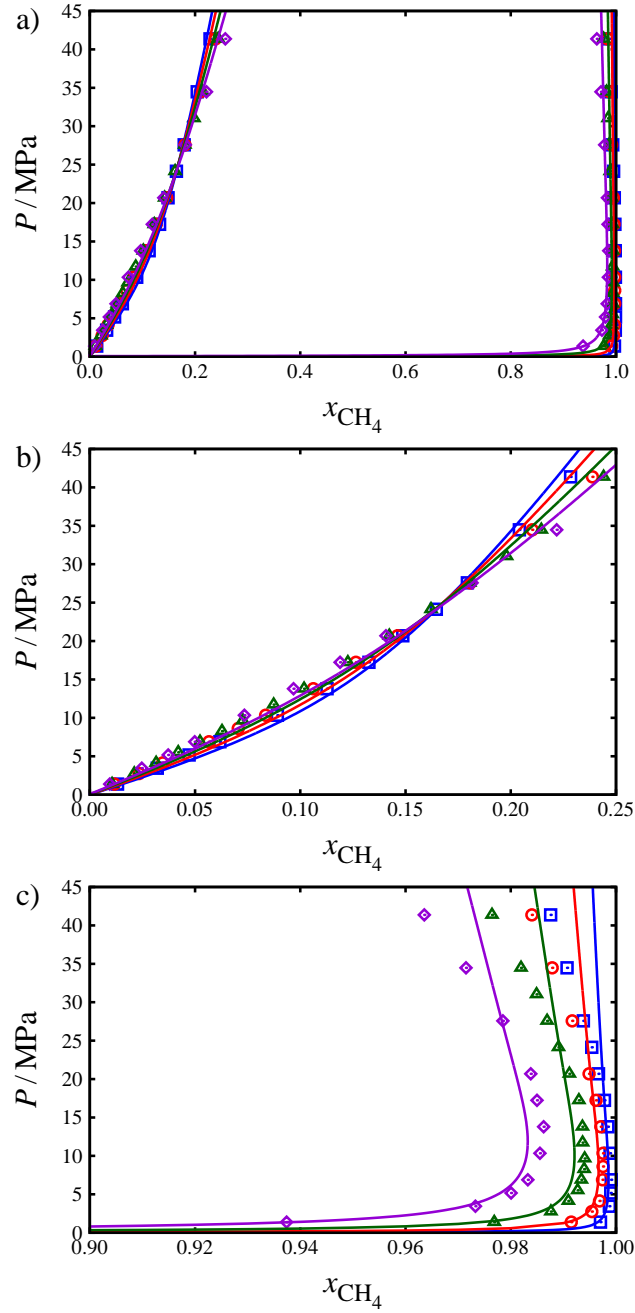
Figure 7: Isothermal pressure-mole fraction (P-x) vapour-liquid and liquid-liquid equilibria of methanol + methane. The symbols represent the experimental data [101] at temperatures of $T = 273.15$ K (squares), $T = 290$ K (circles), $T = 310$ K (triangles), and $T = 330$ K (diamonds), while the continuous curves represent the description with the SAFT-γ Mie approach [13]: (a) global fluid-phase diagram, (b) methanol-rich phase, and (c) methane-rich phase.
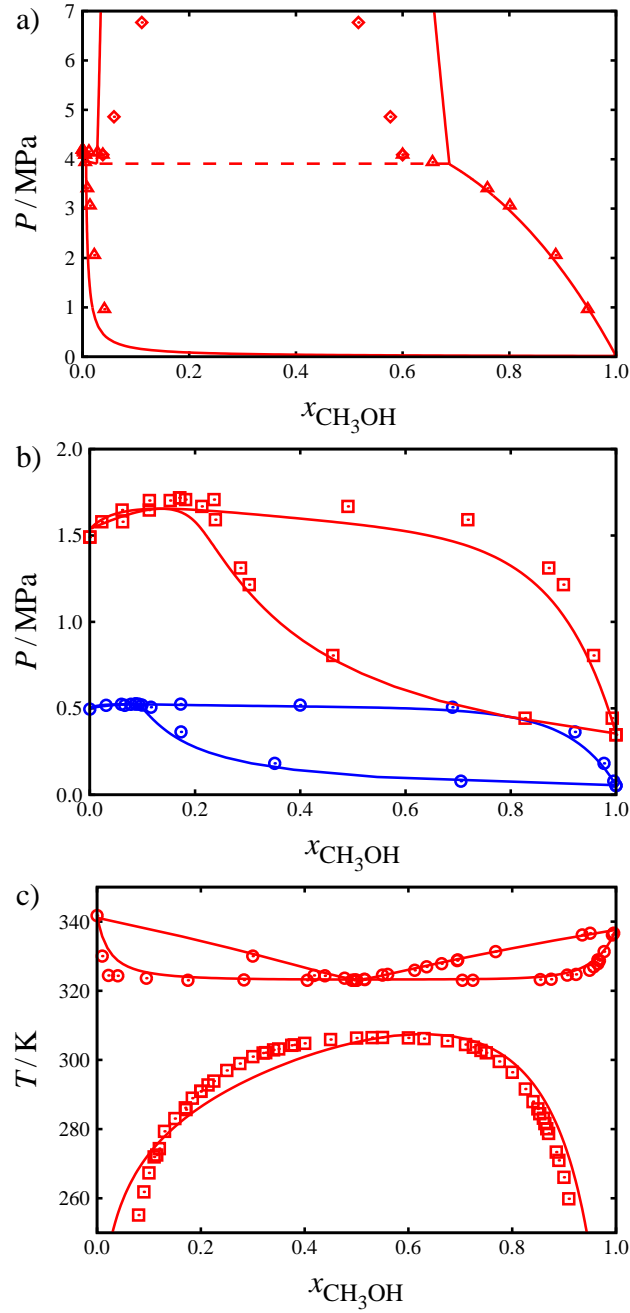
Figure 8: Vapour-liquid and liquid-liquid equilibria of selected binary mixtures of methanol + n-alkanes. The symbols represent the experimental data and the continuous curves the description with the SAFT-γ Mie approach [13]: (a) isothermal pressure-mole fraction (P-x) phase diagram of methanol + ethane [104] at a temperature of $T = 298.15$ K, the triangles represent vapour-liquid equilibrium data, and the diamonds liquid-liquid equilibrium data; (b) isothermal pressure-mole fraction (P-x) phase diagram of methanol + n-butane [105] at temperatures of $T = 323.15$ K (circles), and $T = 373.15$ K (squares); (c) isobaric temperature-mole fraction (T-x) phase diagram of methanol + n-hexane at a pressure of $P = 0.101$ MPa, the circles represent vapour-liquid equilibrium data [102], and the squares liquid-liquid equilibrium data [103].

22

is estimated using experimental phase equilibrium data at 423.15 and 473.15 K [106]; the value of the parameter is reported in Table 3. This parameter is then used to predict the phase equilibrium at other temperatures. The SAFT-γ Mie predictions are compared to experimental data [106] in Figure 9. SAFT-γ Mie provides a good description of the experimental data, with both phases described accurately over a range of temperatures, although the minimum of solubility of methane in the water-rich phase around 340 K is not captured.

The modelling of other n-alkane + water mixtures requires the determination of the CH_3-H_2O and CH_2-H_2O unlike group interactions; the dispersion energies (ε_{kl}) are reported in Table 3. These values are estimated using experimental isobaric ($P = 1$ atm) n-heptane + water phase equilibrium data [108, 109], and can then been used to predict the isothermal phase equilibria of three other n-alkane + water mixtures. The predictions for n-butane + water, n-hexane + water, and n-decane + water are compared with experimental data [110–115] in Figure 10. As can be seen from the figure, the SAFT-γ Mie predictions provide a good overall description of both the VLE and LLE of the three systems considered. The ability to describe the higher (LLE) and lower (VLE) pressure regimes of the mixtures is a stringent test of the model. The SAFT-γ Mie group-contribution method is shown to deliver a very accurate prediction in both regimes; a similarly encouraging result was presented early on with the SAFT-γ square-well methodology [56].

As the alkane + water systems, the carbon dioxide + water binary mixture also exhibits type III fluid-phase behaviour characterized by extension regions of liquid-liquid immiscibility. As mentioned earlier, CO_2 is modelled here including one association site that is inactive except in the presence of water where it interacts with the two e sites of water. Previous works using the Wertheim association theory concluded that such an association scheme was the most suited to describe the fluid-phase behaviour of water + carbon dioxide [61–63]. The determination of the CO_2-H_2O unlike interaction hence involves three unlike parameters: the unlike dispersion energy ($\varepsilon_{CO_2H_2O}$), the unlike association energy ($\varepsilon_{CO_2H_2O,He}^{HB}$), and the unlike association bonding volume ($K_{CO_2H_2O,He}$). These parameters are estimated using experimental phase equilibrium data at 323.2 K [116] and are presented in Table 3. Once these parameters have been prescribed they are used to predict other isotherms. The results of the SAFT-γ Mie predictions are compared with experimental data, as well as with the description obtained using the CPA EoS [3, 117] in Figure 11. We provide a comparison with results obtained with the CPA EoS here instead of the PPR78 as the CPA EoS accounts for the association in the mixture and is hence provides a better point of comparison to assess the quality of our SAFT-γ Mie methodology. It can be seen in the figure that SAFT-γ Mie provides an excellent description of the compositions of both the water-rich and carbon dioxide-rich phases of this challenging mixture, including the minimum of solubility of water in the carbon dioxide-rich phase characteristic of non-azeotropic type III phase behaviour with gas-gas immiscibility of the second kind [100], which is discussed in more detail by Dos Ramos *et al.* [118, 119]. This minimum in solubility is difficult to capture accurately as it requires a good description of the locus of the three-phase line as well as a good agreement with the
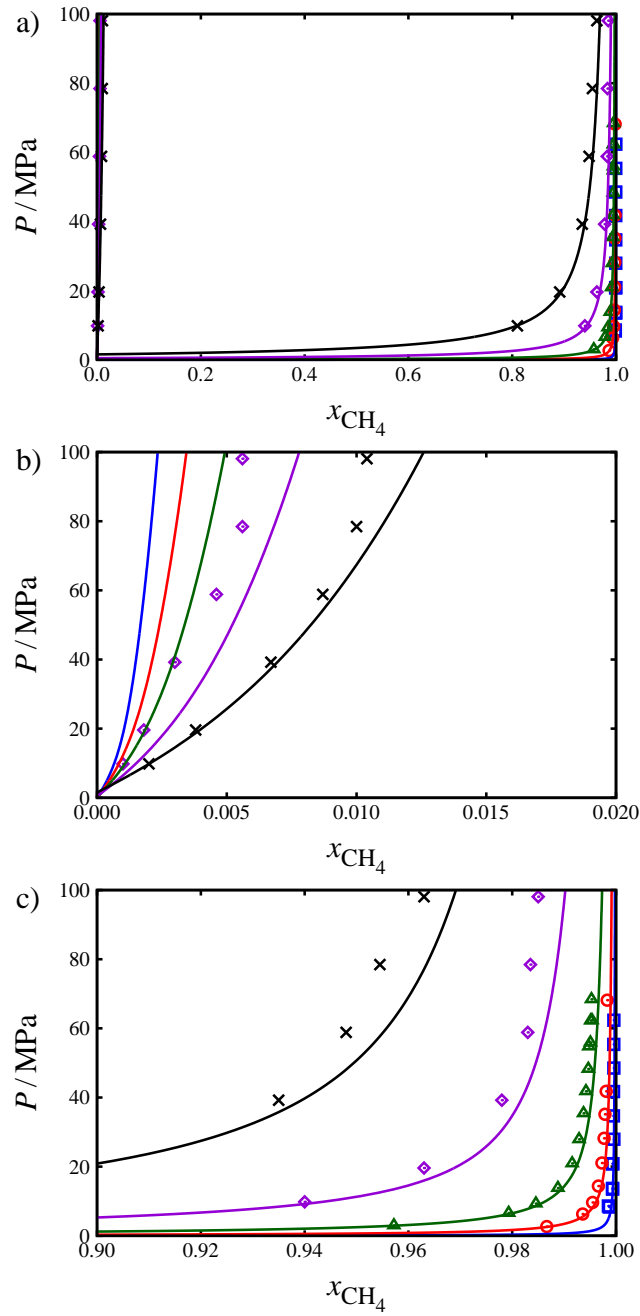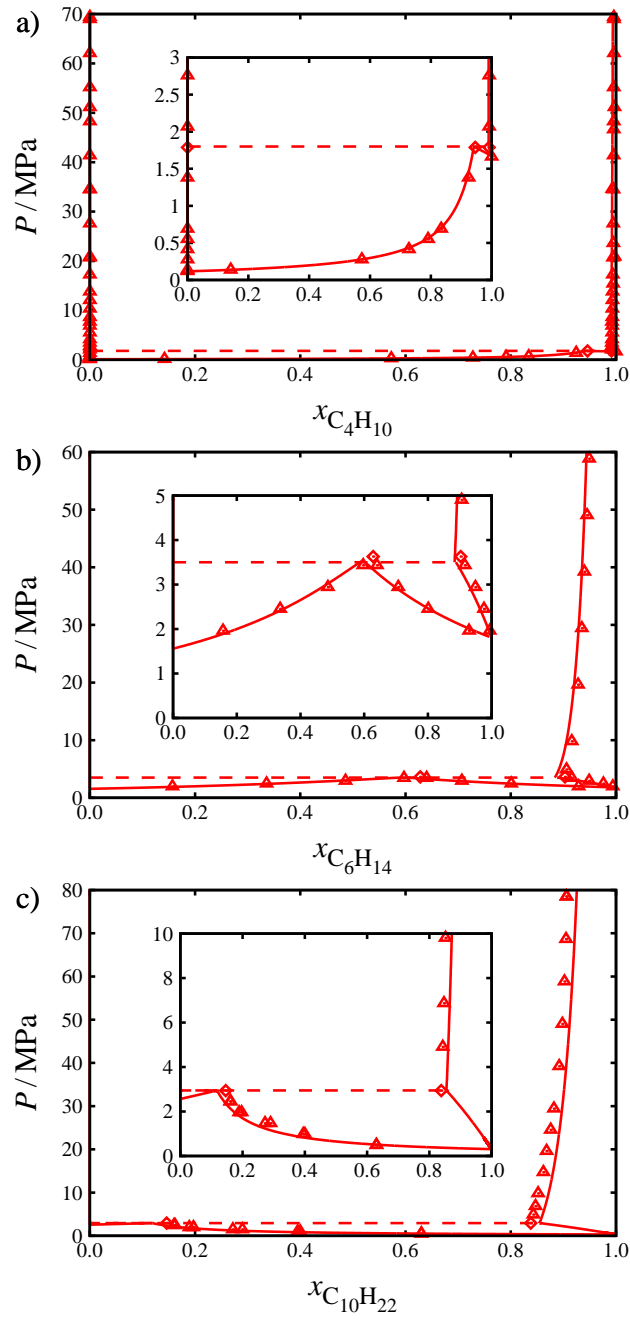
23

Figure 9: Isothermal pressure-mole fraction (P-x) vapour-liquid and liquid-liquid equilibria of water + methane. The symbols represent the experimental data at temperatures of $T = 310.93$ K [107] (squares), $T = 344.26$ K [107] (circles), $T = 377.59$ K [107] (triangles), $T = 423.15$ K [106] (diamonds), and $T = 473.15$ K [106] (crosses), while the continuous curves represent the description with the SAFT-γ Mie approach [13]: (a) entire composition range, (b) water-rich phase, and (c) methane-rich phase.

Figure 10: Isothermal pressure-mole fraction (P-x) vapour-liquid and liquid-liquid equilibria of n-alkanes + water. The symbols represent the experimental data, while the continuous curves represent the predictions with the SAFT-γ Mie approach [13]. The dashed line corresponds to the three-phase (vapour-liquid-liquid) equilibrium pressure. (a) n-butane + water [110–112] at a temperature of $T = 377.59$ K, (b) n-hexane + water [113–115] at a temperature of $T = 473.15$ K, and (c) n-decane + water [113, 114] at a temperature of $T = 498.15$ K.

Table 6: Absolute errors in composition (defined in Eq. 13) for the binary systems presented in Figures 5 to 12.

System	Δx	Δy
Methane + Carbon dioxide	1.11	0.47
Propane + Carbon dioxide	3.20	1.50
n-decane + Carbon dioxide	2.00	0.76
Methane + Methanol	0.23	0.56
Ethane + Methanol	0.08	0.17
n-butane + Methanol	0.16	0.03
n-hexane + Methanol	1.00	0.45
Methane + Water	4.14	2.41
n-butane + Water	7.45	2.10
n-hexane + Water	5.21	2.58
n-decane + Water	0.03	0.33
Carbon Dioxide + Water	3.02	1.38
Methanol + Water	3.44	1.70

high-pressure solubilities.

The Henry's law coefficients and excess enthalpies of mixing for the carbon dioxide + water system are also predicted with the SAFT-γ Mie approach and are compared with experimental data [120–137] in Figure 12. It can be seen that a very good description of the experimental data is obtained in a fully predictive manner.

The water + methanol binary mixture exhibits type I phase behaviour in the classification of van Konynenburg and Scott [100]: only VLE is observed for this mixture. The determination of the CH_3OH-H_2O unlike interaction requires the adjustment of the unlike dispersion energy ε_{kl}, the unlike association energy $\varepsilon_{kl,ab}^{\mathrm{HB}}$, and the unlike association bonding volume $K_{kl,ab}$. A symmetrical association scheme is used: $\varepsilon_{CH_3OH-H_2O,He}^{\mathrm{HB}} = \varepsilon_{CH_3OH-H_2O,eH}^{\mathrm{HB}}$ and $K_{CH_3OH-H_2O,He} = K_{CH_3OH-H_2O,eH}$. These parameters are estimated using experimental VLE data at 0.101 MPa [138], and the resulting parameters are then transferred to the prediction of the isothermal VLE at four temperatures. The results of these predictions are compared with experimental data in Figure 13, where the excellent quality of the description provided by SAFT-γ Mie is apparent.

In addition to the graphical comparisons provided, a summary of the absolute error in composition for the phase equilibria of the binary mixtures examined in this section is provided in Table 6. The small values of these errors confirm the accuracy and predictive capability of the SAFT-γ Mie group-contribution methodology.
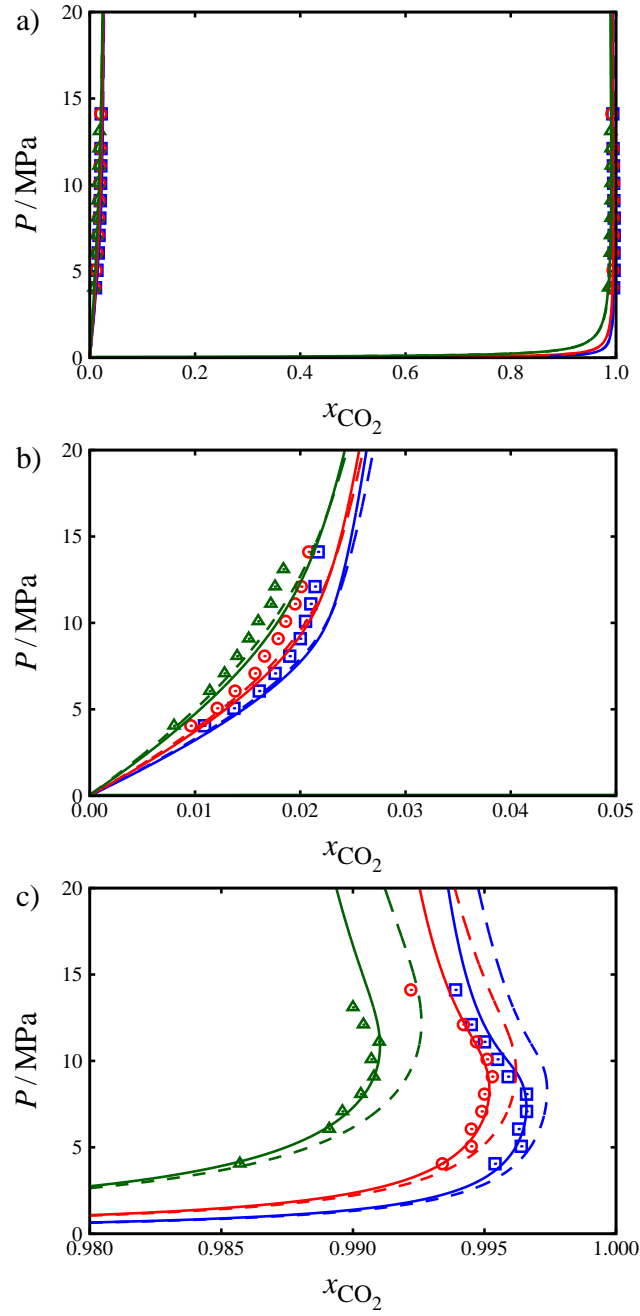
Figure 11: Isothermal pressure-mole fraction (P-x) vapour-liquid and liquid-liquid equilibria of water + carbon dioxide. The symbols represent the experimental data [116] at temperatures of $T = 323.2$ K (squares), $T = 333.2$ K (circles), and $T = 353.1$ K (triangles), while the continuous curves represent the description with the SAFT-γ Mie approach [13], and the dashed curves the description with the CPA equation of state [3, 117]: (a) entire composition range, (b) water-rich phase, and (c) carbon-dioxide-rich phase.
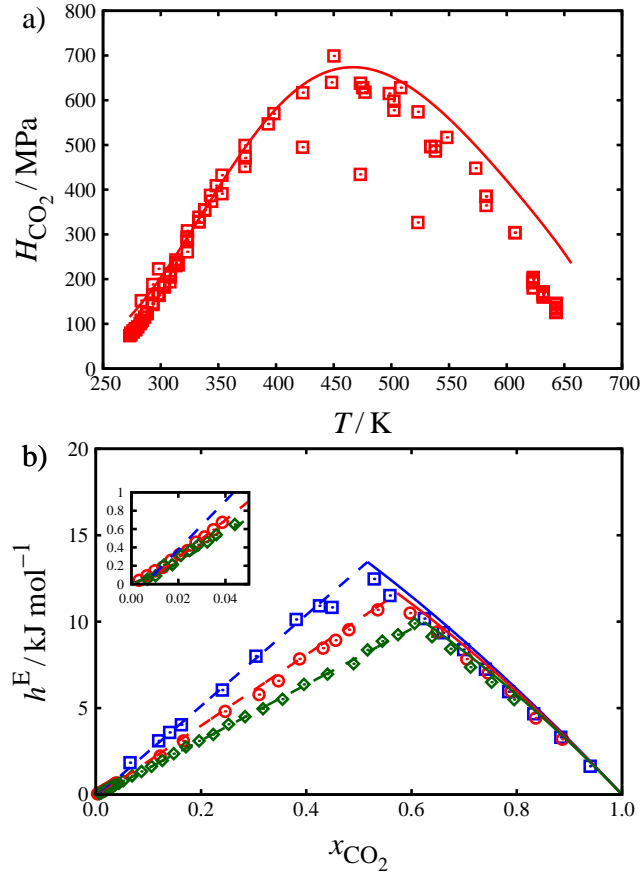
Figure 12: (a) Henry's law coefficients for water + carbon dioxide; the symbols represent the experimental data [120–136] and the continuous curve the prediction of the SAFT-γ Mie approach [13]; (b) Isothermal-isobaric excess molar enthalpy of mixing for water + carbon dioxide. The symbols represent the experimental data [137] at a temperature of $T = 523.15$ K and pressures of $P = 10.4$ MPa (squares), $P = 12.4$ MPa (circles), and $P = 15$ MPa (diamonds); the continuous and dashed curves represent the predictions of the SAFT-γ Mie approach [13] for the one-phase regions and two phase region, respectively.

28
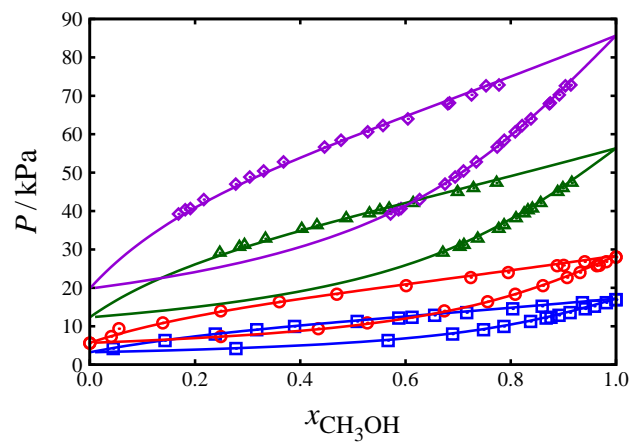
Figure 13: Isothermal pressure-mole fraction (P-x) vapour-liquid equilibria of methanol + water. The symbols represent the experimental data at temperatures of $T = 298.14$ K [139] (squares), $T = 308.15$ K [140] (circles), $T = 323.15$ K [141] (triangles), and $T = 333.15$ K [141] (diamonds), while the continuous curves represent the predictions with the SAFT-γ Mie approach [13].

3.3. Ternary Mixtures

Although ternary mixtures are more complex than binary mixtures and thus a step towards the description of the real fluids encountered in the oil and gas industry that can contain large numbers of components, ternary mixtures are simple enough that experimental data on well-characterized systems are available. As all of the necessary group interactions have been determined from pure components and binary mixtures, ternary mixtures can now be treated without any further parameter estimation, therefore providing a further test of the predictive capabilities of the methodology. To illustrate the performance of the SAFT-γ Mie approach in describing ternary mixtures two systems are chosen: methanol + n-propane + carbon dioxide; and water + methanol + n-hexane.

Three sets of conditions are considered for the methanol + n-propane + carbon dioxide ternary mixture: $T = 313.1$ K - $P = 1.21$ MPa; $T = 343.1$ K - $P = 1.21$ MPa; and $T = 343.1$ K - $P = 2.7$ MPa. At these conditions the methanol + carbon dioxide binary mixture exhibits a wide fluid-fluid immiscibility gap. For both temperatures at the lower pressure the methanol + n-propane binary mixture exhibits vapour-liquid phase equilibria while carbon dioxide and n-propane are fully miscible. As a result, for both temperatures at the lower pressure considered, the fluid-phase behaviour of the ternary mixture is characterized by a two-phase region, with the phase boundaries extending from the methanol + carbon dioxide binary mixture to the methanol + n-propane mixture VLE boundary. At the higher temperature and pressure considered methanol and n-propane are miscible [142], while the carbon dioxide + n-propane mixture exhibits a small vapour-liquid region close to pure n-propane (although no experimental data are available, the pressure is slightly above the vapour pressure of propane and a simple extrapolation of the data of Reamer *et al.* [143] leads to a phase split at these conditions). The phase behaviour of the ternary mixture, while still characterized by a two-phase region, reflects the change in the phase behaviour of the constituent binary mixtures, with the phase boundaries now extending from the methanol + carbon dioxide binary mixture phase boundaries to those of the carbon dioxide + n-propane binary mixture. The experimental data [142] for this system are compared with the SAFT-γ Mie predictions in Figure 14(a). It can be seen from the figure that the SAFT-γ Mie predictions are in good agreement with the data and capture this change in phase behaviour very well.

The second ternary mixture considered in our current work is water + methanol + n-hexane at $T = 318.15$ K and $P = 0.101$ MPa. As mentioned in the previous section the water + n-hexane binary mixture exhibits an extensive liquid-liquid region under these conditions, while methanol is fully miscible with both water and n-hexane at these conditions. This leads to the appearance of a broad two-phase region in the ternary mixture with methanol partitioning between a water-rich phase and a n-hexane-rich phase, a feature common to ternary mixtures containing water, an alkane and a small polar molecule. The comparison between the experimental data [144] and the SAFT-γ Mie predictions provided in Figure 14(b) highlights the fidelity of the approach in reproducing the experimental phase envelope and tie-lines. The quality of the predicted calculations is better appreciated studying the corresponding K values for the two ternary

systems; these are presented in Figure 15. For the methanol + propane + carbon dioxide system the K value of propane is calculated as

$$K_{\mathrm{C_3H_8}} = \frac{y_{\mathrm{C_3H_8}}}{x_{\mathrm{C_3H_8}}} \; , \tag{14}$$

and a comparison of the experimental and calculated values for a given composition of propane in the gas phase $y_{\mathrm{C_3H_8}}$ is provided. For the water + methanol + n-hexane mixture the K value of methanol is calculated as

$$K_{\mathrm{CH_3OH}} = \frac{x^{WR}_{\mathrm{CH_3OH}}}{x^{HR}_{\mathrm{CH_3OH}}} \; , \tag{15}$$

where the superscripts WR and HR indicate the water-rich and n-hexane-rich phases, respectively. A comparison of the experimental and calculated values for a given $x^{HR}_{\mathrm{CH_3OH}}$ is given in the figure. It is apparent that, with the exception of a small number of points (corresponding to the higher temperature and pressure states of the propane + carbon dioxide + methanol system and to the region of very low methanol content for the water + n-hexane + methanol system) the calculated values are in good agreement with the experimental data.

4. Conclusion

The application of the SAFT-γ Mie group-contribution approach [13] to selected mixtures with components relevant to the oil and gas industry is shown to provide an excellent description of the properties for the systems of interest. Pure-component coexistence properties are reproduced well with our method, and single-phase densities and second-derivative properties are predicted with excellent accuracy. Several of the compounds considered here have been modelled using molecular groups due to their small size. Others have been described with representative chemical functional groups, making it possible to make use of the advantage conferred to SAFT-γ Mie by its heterogroup nature, which allows one to obtain unlike group interactions from pure-component data alone. The capability of SAFT-γ Mie to give exceptional predictions of the fluid-phase behaviour of binary mixtures of families of compounds based on interactions developed using data for only a few of the members of the family is demonstrated on an extensive set of mixtures and highlights the versatility of the group-contribution methodology. The predictive capability of the SAFT-γ Mie approach also extends to the treatment of mixtures at different conditions and of other properties. The use of association sites within the underlying SAFT base of the approach enables a high quality treatment of hydrogen-bonding and polar fluids, such as water, carbon dioxide, methanol, and mixtures containing these species. The SAFT-γ Mie approach provides good descriptions of the VLE and LLE for the systems of interest, including challenging phenomena such as the solubility minimum of water in the carbon-dioxide-rich phase and the crossing point of the isotherms of the methane solubility in the methanol-rich phase. Furthermore, second-derivative properties and excess properties of mixing are also described well, making SAFT-γ Mie a promising generic platform for thermodynamic modelling in the oil and gas industry. In our
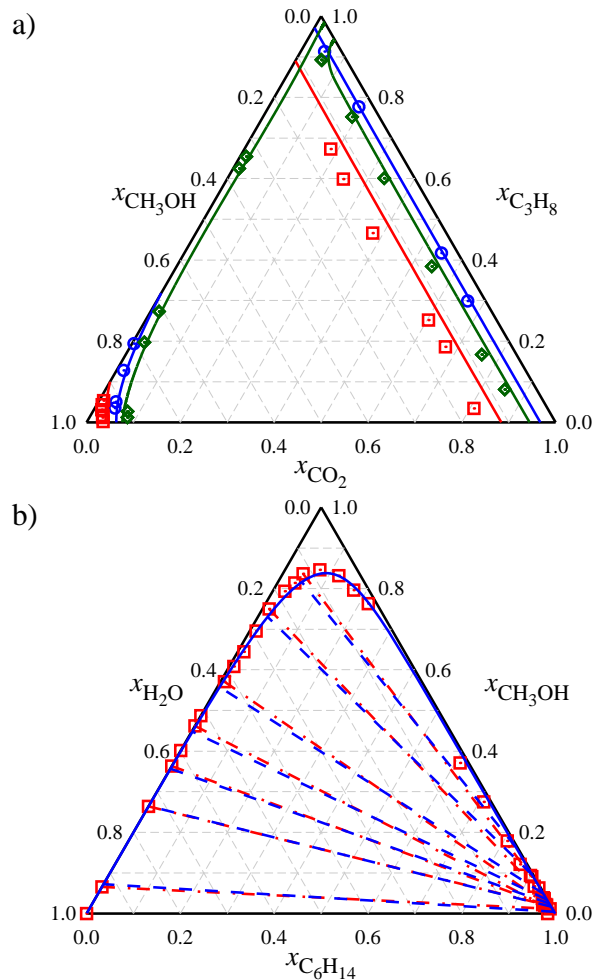
Figure 14: Isothermal-isobaric fluid-phase equilibrium of ternary mixtures. The symbols represent the experimental data and the continuous curves the predictions of the SAFT-γ Mie approach [13]: (a) Propane + carbon dioxide + methanol [142] at temperatures and pressures of $T = 313.1$ K - $P = 1.21$ MPa (circles), $T = 343.1$ K - $P = 1.21$ MPa (squares), and $T = 343.1$ K - $P = 2.7$ MPa (diamonds); (b) Water + n-hexane + methanol at a temperature of $T = 318.15$ K and a pressure of $P = 0.101$ MPa [144], the dash dotted lines and the dashed lines represent the experimental and predicted tie lines, respectively;.
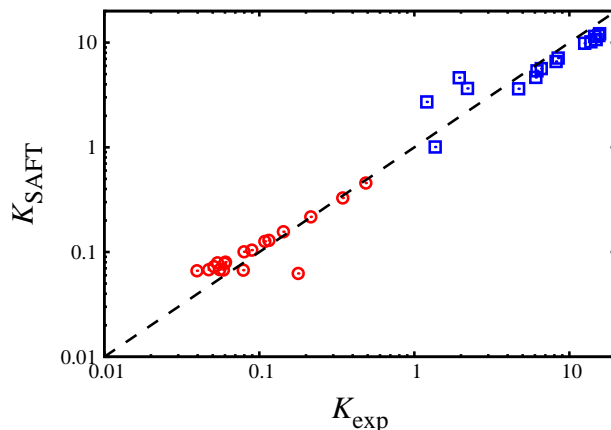
Figure 15: Experimental versus calculated K values for the ternary mixtures propane + carbon dioxide + methanol (squares) and water + n-hexane + methanol (circles).

current work new groups, including CO_2, CH_3OH, aCH, aCCH$_2$, and aCCH$_3$, and group-group interactions have been characterized. As the table of available interactions continues to expand, an increasingly large number of mixtures becomes accessible. In future work we will continue testing the performance of the method on an increasing set of systems. The intermolecular parameters obtained with the SAFT-γ Mie methodology can also be used directly with molecular dynamics simulation to provide a route to structural, interfacial and dynamical properties that are not directly accessible from the equation of state enhancing the predictive capabilities of the methodology [145–150].

Acknowledgements

Data underlying this article can be accessed on Zenodo at https://zenodo.org/record/ XXXXXXXXX, and used under the Creative Commons Attribution licence.

[1] D. Y. Peng and D. B. Robinson, Ind. Eng. Chem. Fundam. **15**, 59 (1976).

[2] G. Soave, Chem. Eng. Sci. **27**, 1197 (1972).

[3] G. M. Kontogeorgis, E. Voutsas, I. V. Yakoumis, and D. P. Tassios, Ind. Eng. Chem. Res. **35**, 4310 (1996).

[4] W. G. Chapman, K. E. Gubbins, G. Jackson, and M. Radosz, Fluid Phase Equilib. **52**, 31 (1989).

[5] W. G. Chapman, K. E. Gubbins, G. Jackson, and M. Radosz, Ind. Eng. Chem. Res. **29**, 1709 (1990).

[6] J.-N. Jaubert and R. Privat, Fluid Phase Equilib. **295**, 26 (2010).

[7] J. N. Jaubert and F. Mutelet, Fluid Phase Equilib. **224**, 285 (2004).

[8] S. Tamouza, J. P. Passarello, P. Tobaly, and J. C. de Hemptinne, Fluid Phase Equilib. **222-223**, 67 (2004).

[9] A. Lymperiadis, C. S. Adjiman, A. Galindo, and G. Jackson, J. Chem. Phys. **127**, 234903 (2007).

[10] A. Lymperiadis, C. S. Adjiman, G. Jackson, and A. Galindo, Fluid Phase Equilib. **274**, 85 (2008).

[11] Y. Peng, K. D. Goff, M. C. dos Ramos, and C. McCabe, Fluid Phase Equilib. **277**, 131 (2009).

[12] K. Paduszyński and U. Domańska, Ind. Eng. Chem. Res. **51**, 12967 (2012).

[13] V. Papaioannou, T. Lafitte, C. Avendaño, C. S. Adjiman, G. Jackson, E. A. Müller, and A. Galindo, J. Chem. Phys. **140**, 054107 (2014).

[14] W. B. Whiting, J. Chem. Eng. Data **41**, 935 (1996).

[15] R. Dohrn and O. Pfohl, Fluid Phase Equilib. **194-197**, 15 (2002).

[16] E. D. Sloan and C. A. Koh, *Clathrate Hydrates of Natural Gases* (CRC Press, Boca Raton, 2008), 3rd ed.

[17] J. V. Sengers and J. M. H. Levelt Sengers, Ann. Rev. Phys. Chem. **37**, 189 (1986).

[18] G. M. Kontogeorgis and G. K. Folas, *Thermodynamic models for industrial applications. From classical and advanced mixing rules to association theories* (Wiley, UK, 2010).

[19] O. Redlich, E. L. Derr, and G. J. Pierotti, J. Am. Chem. Soc. **81**, 2283 (1959).

[20] G. Jackson, W. G. Chapman, and K. E. Gubbins, Mol. Phys. **65**, 1 (1988).

[21] W. G. Chapman, G. Jackson, and K. E. Gubbins, Mol. Phys. **65**, 1057 (1988).

[22] A. Danesh, D.-H. Xu, and A. Todd, Fluid Phase Equilib. **63**, 259 (1991).

[23] H. Li and J. Yan, Appl. Energy **86**, 826 (2009).

[24] A. Peneloux, E. Rauzy, and R. Freze, Fluid Phase Equilib. **8**, 7 (1982).

[25] S. Vitu, R. Privat, J. N. Jaubert, and F. Mutelet, J. Supercrit. Fluids **45**, 1 (2008).

[26] J.-W. Qian, R. Privat, and J.-N. Jaubert, Ind. Eng. Chem. Res. **52**, 16457 (2013).

[27] T. S. Khasanshin, A. P. Shchamialiou, and O. G. Poddubskij, Int. J. Thermophys. **24**, 1277 (2003).

[28] A. Galindo, P. J. Whitehead, G. Jackson, and A. N. Burgess, J. Phys. Chem. **100**, 6781 (1996).

[29] G. M. Kontogeorgis, I. V. Yakoumis, H. Meijer, E. Hendriks, and T. Moorwood, Fluid Phase Equilib. **158-160**, 201 (1999).

[30] E. C. Voutsas, G. C. Boulougouris, I. G. Economou, and D. P. Tassios, Ind. Eng. Chem. Res. **39**, 797 (2000).

[31] B. H. Patel, P. Paricaud, A. Galindo, and G. C. Maitland, Ind. Eng. Chem. Res. **42**, 3809 (2003).

[32] X. S. Li and P. Englezos, Fluid Phase Equilib. **224**, 111 (2004).

[33] L. F. Vega, F. Llovell, and F. J. Blas, J. Phys. Chem. B **113**, 7621 (2009).

[34] J. M. Miguez, M. C. dos Ramos, M. M. Piñeiro, and F. J. Blas, J. Phys. Chem. B **115**, 9604 (2011).

[35] S. Z. S. Al Ghafri, E. Forte, G. C. Maitland, J. J. Rodriguez-Henriquez, and J. P. M. Trusler, J. Phys. Chem. B **118**, 14461 (2014).

[36] C. McCabe and G. Jackson, Phys. Chem. Chem. Phys. **1**, 2057 (1999).

[37] P. Paricaud, A. Galindo, and G. Jackson, Ind. Eng. Chem. Res. **43**, 6871 (2004).

[38] G. H. Hudson and J. C. McCoubrey, Trans. Faraday Soc. **56**, 761 (1960).

[39] A. J. Haslam, A. Galindo, and G. Jackson, Fluid Phase Equilib. **266**, 105 (2008).

[40] M. Hajiw, A. Chapoy, and C. Coquelet, Can. J. Chem. Eng. **93**, 432 (2015).

[41] H. P. Gros, S. Bottini, and E. A. Brignole, Fluid Phase Equilib. **116**, 537 (1996).

[42] T. M. Soria, F. A. Sánchez, S. Pereda, and S. B. Bottini, Fluid Phase Equilib. **296**, 116 (2010).

[43] T. Lafitte, A. Apostolakou, C. Avendaño, A. Galindo, C. S. Adjiman, E. A. Müller, and G. Jackson, J. Chem. Phys. **139**, 154504 (2013).

[44] T. Lafitte, D. Bessieres, M. M. Piñeiro, and J. L. Daridon, J. Chem. Phys. **124**, 024509 (2006).

[45] T. Lafitte, M. M. Piñeiro, J. L. Daridon, and D. Bessieres, J. Phys. Chem. B **111**, 3447 (2007).

[46] S. Dufal, T. Lafitte, A. J. Haslam, A. Galindo, G. N. I. Clark, C. Vega, and G. Jackson, Mol. Phys. **113**, 948 (2015).

[47] S. Dufal, T. Lafitte, A. Galindo, G. Jackson, and A. J. Haslam, AIChE Journal **61**, 2891 (2015).

[48] S. Dufal, V. Papaioannou, M. Sadeqzadeh, T. Pogiatzis, A. Chremos, C. S. Adjiman, G. Jackson, and A. Galindo, J. Chem. Eng. Data **59**, 3272 (2014).

[49] G. Mie, Ann. Phys. **316**, 657 (1903).

[50] E. A. Grüneisen, Z. Elektrochem. Angew. Phys. Chem. **17**, 737 (1911).

[51] E. A. Grüneisen, Ann. Phys. **344**, 257 (1912).

[52] J. E. Jones, Proc. Roy. Soc. London A **106**, 441 (1924).

[53] J. E. Jones, Proc. Roy. Soc. London A **106**, 463 (1924).

[54] J. E. Lennard-Jones, Proc. Phys. Soc. **43**, 461 (1931).

[55] PSE Ltd., gPROMS v. 3.4.0 (2011), http://www.psenterprise.com/.

[56] V. Papaioannou, C. S. Adjiman, G. Jackson, and A. Galindo, Fluid Phase Equilib. **306**, 82 (2011).

[57] M. C. dos Ramos, J. D. Haley, J. R. Westwood, and C. McCabe, Fluid Phase Equilib. **306**, 97 (2011).

[58] F. E. Pereira, G. Jackson, A. Galindo, and C. S. Adjiman, Fluid Phase Equilib. **299**, 1 (2010).

[59] E. P. J. Linstrom and W. G. Mallard, NIST *Chemistry WebBook,* NIST *Standard Reference Database Number 69* (National Institutes of Standards and Technology WebBook, Gaithersburg MD, 20899, 2013).

[60] M. Sadeqzadeh, V. Papaioannou, S. Dufal, C. S. Adjiman, G. Jackson, and A. Galindo, Fluid Phase Equilib. **407**, 39 (2016).

[61] G. M. Kontogeorgis, M. L. Michelsen, G. K. Folas, S. Derawi, N. von Solms, and E. H. Stenby, Ind. Eng. Chem. Res. **45**, 4869 (2006).

[62] R. Sun and J. Dubessy, Geochim. Cosmochim. Acta **74**, 1982 (2010).

[63] I. Tsivintzelis, G. M. Kontogeorgis, M. L. Michelsen, and E. H. Stenby, Fluid Phase Equilib. **306**, 38 (2011).

[64] N. Allemand, J. Jose, and J. C. Merlin, Thermochim. Acta **105**, 79 (1986).

[65] D. Ambrose, J. Chem. Thermodyn. **19**, 1007 (1987).

[66] C. A. Buehler, T. S. Gardner, and M. L. Clemens, J. Org. Chem. **2**, 167 (1937).

[67] D. L. Camin, A. D. Forziati, and F. D. Rossini, J. Phys. Chem. **58**, 440 (1954).

[68] E. B. Evans, J. Inst. Pet. Technol. **24**, 537 (1938).

[69] A. F. Forziati, W. R. Norris, and F. D. Rossini, J. Res. Natl. Bur. Stand. **43**, 555 (1949).

[70] J. L. Hales and R. Townsend, J. Chem. Thermodyn. **4**, 763 (1972).

[71] E. C. Ihmels, *Viscosity measurements with a ubbelohde-viscosimeter and density measurements with a resonance frequency transducer prototype*, Diplomarbeit (1998), (cited in DETHERM).

[72] T. Y. Ju, G. Shen, and C. E. Wood, J. Inst. Pet. **26**, 514 (1940).

[73] H. Kasehgari, I. Mokbel, C. Viton, and J. Jose, Fluid Phase Equilib. **87**, 133 (1993).

[74] T. Kimura, T. Matsushita, and T. Kamiyama, J. Solution Chem. **33**, 875 (2004).

[75] G. Liessmann, W. Schmidt, and S. Reiffarth, Data compilation of the Saechsische Olefinwerke Boehlen Germany (1995), (cited in DETHERM).

[76] J. Linek, V. Fried, and J. Pick, Collect. Czech. Chem. Commun. **30**, 1358 (1965).

[77] I. Mokbel, E. Rauzy, J. P. Meille, and J. Jose, Fluid Phase Equilib. **147**, 271 (1998).

[78] J. Ortega, G. Bolat, and E. Marrero, Phys. Chem. Liq. **45**, 251 (2007).

[79] V. Ruzicka, M. Zabransky, K. Ruzicka, and V. Majer, Thermochim. Acta **245**, 121 (1994).

[80] P. M. Sherblom, P. M. Gschwend, and R. P. Eganhouse, J. Chem. Eng. Data **37**, 394 (1992).

[81] W. V. Steele, R. D. Chirico, S. E. Knipmeyer, and A. Nguyen, J. Chem. Eng. Data **47**, 648 (2002).

[82] N. B. Vargaftik, *Handbook of thermophysical properties of gases and fluids* (Nauka, Moscow, 1972).

[83] S. P. Verevkin, J. Chem. Thermodyn. **38**, 1111 (2006).

[84] Z. W. Yu, X. H. He, R. Zhou, Y. Liu, and X. D. Sun, Fluid Phase Equilib. **164**, 209 (1999).

[85] D. Jain and N. Dhar, Fluid Phase Equilib. **47**, 89 (1989).

[86] K. Hsu and H. Clever, J. Chem. Thermodyn. **7**, 435 (1975).

[87] S. Murakami, V. Lam, and G. Benson, J. Chem. Thermodyn. **1**, 397 (1969).

[88] M. M. Miller and K. D. Luks, Fluid Phase Equilib. **44**, 295 (1989).

[89] G. M. Schneider, J. Supercrit. Fluids **13**, 5 (1998).

[90] T. A. Al-Sahhaf, A. J. Kidnay, and E. D. Sloan, Ind. Eng. Chem. Fundam. **22**, 372 (1983).

[91] M. S. W. Wei, T. S. Brown, A. J. Kidnay, and E. D. Sloan, J. Chem. Eng. Data **40**, 726 (1995).

[92] H. H. Reamer and B. H. Sage, J. Chem. Eng. Data **8**, 508 (1963).

[93] G. Besserer and D. Robinson, J. Chem. Eng. Data **18**, 416 (1973).

[94] J. H. Kim and M. S. Kim, Fluid Phase Equilib. **238**, 13 (2005).

[95] J. J. Christensen, P. W. Faux, D. Cordray, and R. M. Izatt, J. Chem. Thermodyn. **18**, 1053 (1986).

[96] W. K. Tolley, R. M. Izatt, and J. L. Oscarson, Thermochim. Acta **181**, 127 (1991).

[97] B. Bian, Ph.D. thesis, University of Nanjing, Nanjing (1992).

[98] E. Brunner, J. Chem. Thermodyn. **17**, 871 (1985).

[99] I. Hölscher, G. Schneider, and J. Ott, Fluid Phase Equilib. **27**, 153 (1986).

[100] P. H. van Konynenburg and R. L. Scott, Philos. Trans. R. Soc., A **298**, 495 (1980).

[101] J. H. Hong, P. V. Malone, M. D. Jett, and R. Kobayashi, Fluid Phase Equilib. **38**, 83 (1987).

[102] J. D. Raal, R. K. Code, and D. A. Best, J. Chem. Eng. Data **17**, 211 (1972).

[103] G. Hradetzky and H. J. Bittrich, Int. Data Series, Selected Data on Mixtures, Ser. A pp. 216–218 (1986).

[104] K. Ishihara, H. Tanaka, and M. Kato, Fluid Phase Equilib. **144**, 131 (1998).

[105] A. D. Leu, C. J. Chen, and D. B. Robinson, AIChE Symp. Ser. **85**, 11 (1989).

[106] R. G. Sultanov, V. G. Skripka, and A. Y. Namiot, Deposited Doc. VINITI **4386-72**, 1 (1972), (cited in DETHERM).

[107] R. H. Olds, B. H. Sage, and W. N. Lacey, Ind. Eng. Chem. **34**, 1223 (1942).

[108] J. Polak and B. C.-Y. Lu, Can. J. Chem. **51**, 4018 (1973).

[109] M. Freire, L. Gomes, L. Santos, I. Marrucho, and J. Coutinho, J. Phys. Chem. B **110**, 22923 (2006).

[110] H. H. Reamer, R. H. Olds, B. H. Sage, and W. N. Lacey, Ind. Eng. Chem. **36**, 381 (1944).

[111] H. H. Reamer, B. H. Sage, and W. N. Lacey, Ind. Eng. Chem. **44**, 609 (1952).

[112] W. Brooks, G. Gibbs, and J. McKetta, Petro. Refin. **30**, 118 (1951).

[113] A. Y. Namiot, V. G. Skripka, and G. Y. Lotter, Deposited Doc. VINITI **1213-76**, 1 (1976), (cited in DETHERM).

[114] R. G. Sultanov and V. G. Skripka, Deposited Doc. VINITI **4386-72**, 1 (1972), (cited in DETHERM).

[115] R. G. Sultanov and V. G. Skripka, Deposited Doc. VINITI **2347-73**, 1 (1973), (cited in DETHERM).

[116] A. Bamberger, G. Sieder, and G. Maurer, J. Supercrit. Fluids **17**, 97 (2000).

[117] Infochem Computer Services Ltd., Multiflash v. 4.3 (2013), http://www.kbcat.com/.

[118] M. C. dos Ramos, F. J. Blas, and A. Galindo, Fluid Phase Equilib. **261**, 359 (2007).

[119] M. C. dos Ramos, F. J. Blas, and A. Galindo, J. Phys. Chem. C **111**, 15924 (2007).

[120] M. Postigo and M. Katz, J. Solution Chem. **16**, 1015 (1987).

[121] D. Hagewiesche, S. Ashour, and O. Sandall, J. Chem. Eng. Data **40**, 627 (1995).

[122] L. Lizano, M. Lopez, F. Royo, and J. Urieta, J. Solution Chem. **19**, 721 (1990).

[123] E. Wilhelm, R. Battino, and R. Wilcock, Chem. Rev. **77**, 219 (1977).

[124] J. Tokunaga, J. Chem. Eng. Data **20**, 41 (1975).

[125] J. Foussard, P. Reilhac, F. Cammas, and H. Debellefontaine, High Temp. High Pressures **30**, 43 (1998).

[126] W. Su, D. Wong, and M. Li, J. Chem. Eng. Data **54**, 1951 (2009).

[127] G. Schulze and J. Prausnitz, Ind. Eng. Chem. Fundam. **2**, 175 (1981).

[128] D. Zheng, T. Guo, and H. Knapp, Fluid Phase Equilib. **129**, 197 (1997).

[129] M. Malegaonkar, P. Dholabhai, and P. Bishnoi, Can. J. Chem. Eng. **75**, 1090 (1997).

[130] A. Dhima, J. de Hemptinne, and J. Jose, Ind. Eng. Chem. Res. **38**, 3144 (1999).

[131] G. Anderson, J. Chem. Eng. Data **47**, 219 (2002).

[132] J. Kiepe, S. Horstmann, K. Fischer, and J. Gmehling, Ind. Eng. Chem. Res. **41**, 4393 (2002).

[133] I. Dalmolin, E. Skovroinski, A. Biasi, M. Corazza, C. Dariva, and J. Oliveira, Fluid Phase Equilib. **245**, 193 (2006).

[134] C. Dell'Era, P. Uusi-Kyyny, J. Pokki, M. Pakkanen, and V. Alopaeus, Fluid Phase Equilib. **293**, 101 (2010).

[135] A. Ellis and R. Golding, Am. J. Sci. **261**, 47 (1963).

[136] R. Crovetto, R.;Wood, Fluid Phase Equilib. **74**, 271 (1992).

[137] X. Chen, S. Gillespie, J. Oscarson, and R. Izatt, J. Solution Chem. **21**, 825 (1992).

[138] V. Olevskii and I. Golub'ev, Tr. Gos. Nauchno Issled. Proektn. Inst. Azotn. Promst. Prod. Org. Sin. **4**, 36 (1954).

[139] Z. S. Koner, R. C. Phutela, and D. V. Fenby, Aust. J. Chem. **33**, 9 (1980).

[140] M. L. McGlashan and A. G. Williamson, J. Chem. Eng. Data **21**, 196 (1976).

[141] K. Kurihara, T. Minoura, K. Takeda, and K. Kojima, J. Chem. Eng. Data **40**, 679 (1995).

[142] F. Galivel-Solastiouk, S. Laugier, and D. Richon, Fluid Phase Equilib. **28**, 73 (1986).

[143] H. H. Reamer, B. H. Sage, and W. N. Lacey, Ind. Eng. Chem. **43**, 2515 (1951).

[144] J. Liu, Z. Qin, and J. Wang, J. Chem. Eng. Data **47**, 1243 (2002).

[145] C. Avendaño, T. Lafitte, A. Galindo, C. S. Adjiman, G. Jackson, and E. A. Müller, J. Phys. Chem. B **115**, 11154 (2011).

[146] C. Avendaño, T. Lafitte, C. S. Adjiman, A. Galindo, E. A. Müller, and G. Jackson, J. Phys. Chem. B **117**, 2717 (2013).

[147] T. Lafitte, C. Avendaño, V. Papaioannou, A. Galindo, C. S. Adjiman, G. Jackson, and E. A. Müller, Mol. Phys. **110**, 1189 (2012).

[148] O. Lobanova, C. Avendaño, T. Lafitte, E. A. Müller, and G. Jackson, Mol. Phys. **113**, 1228 (2015).

[149] S. Rahman, O. Lobanova, C. Braga, V. Raptis, E. A. Müller, G. Jackson, and A. Galindo, J. Phys. Chem. B, to be submitted p. 25 (2016).

[150] O. Lobanova, A. Mejía, E. A. Müller, and G. Jackson, J. Chem. Thermodynamics **93**, 320 (2016).